

Mechanistic inhibition of gastric cancer-associated bacteria *Helicobacter pylori* by selected phytochemicals: A new cutting-edge computational approach

Shopnil Akash^{a,*}, Imren Bayıl^b, Sajjat Mahmood^c, Nobendu Mukerjee^{d,e,f}, Tamanna Akter Mili^g, Kuldeep Dhama^h, Md Anisur Rahmanⁱ, Swastika Maitra^j, Mohamed Mohany^k, Salim S. Al-Rejaie^k, Nemat Ali^k, Prabhakar Semwal^l, Rohit Sharma^{m,**}

^a Department of Pharmacy, Faculty of Allied Health Sciences, Daffodil International University, Birulia, 1216, Ashulia, Dhaka, Bangladesh

^b Department of Bioinformatics and Computational Biology, Gaziantep University, Turkey

^c Department of Microbiology, Jagannath University, Chittaranjan Avenue in Sadarghat, Dhaka, 1100, Bangladesh

^d Center for Global Health Research, Saveetha Medical College and Hospital, Saveetha Institute Of Medical and Technical Sciences, Chennai, India

^e Department of Microbiology, West Bengal State University, West Bengal, Kolkata, 700126, India

^f Department of Health Sciences, Novel Global Community Educational Foundation, Hebersham, NSW, Australia

^g Department of Pharmacy, University of Asia Pacific, 74/A Green Rd, Dhaka, 1205, Bangladesh

^h Division of Pathology, ICAR-Indian Veterinary Research Institute (IVRI), Izatnagar, 243122, Bareilly, Uttar Pradesh, India

ⁱ Department of Pharmacy, Islamic University, Kushtia, Bangladesh

^j Department of Microbiology, Adamas University, West Bengal, Kolkata, 700126, India

^k Department of Pharmacology and Toxicology, College of Pharmacy, King Saud University, P.O. Box 55760, Riyadh, 1145, Saudi Arabia

^l Department of Biotechnology, Graphic Era University, Dehradun, Uttarakhand, 248002, India

^m Department of Rasa Shastra and Bhaishajya Kalpana, Faculty of Ayurveda, Institute of Medical Science, Banaras Hindu University, Varanasi, 221005, India

ARTICLE INFO

Keywords:

Gastric cancer
Helicobacter pylori
Binding free energy
Drug design
Phytochemicals
Molecular docking
Molecular dynamic simulation
And PCA

ABSTRACT

Background: *Helicobacter pylori* (*H. pylori*) is a persistent bacterial inhabitant in the stomachs of approximately half the global populace. This bacterium is directly linked to chronic gastritis, leading to a heightened risk of duodenal and gastric ulcer diseases, and is the predominant risk factor for gastric cancer - the second most common cause of cancer-related deaths globally. The increasing prevalence of antibiotic resistance necessitates the exploration of innovative treatment alternatives to mitigate the *H. pylori* menace.

Methods: Initiating our study, we curated a list of thirty phytochemicals based on previous literature and subjected them to molecular docking studies. Subsequently, eight phytochemicals—Glabridin, Isoliquiritin, Sanguinarine, Liquiritin, Glycyrrhetic acid, Beta-carotin, Diosgenin, and Sarsasapogenin—were meticulously chosen based on superior binding scores. These were further subjected to an extensive computational analysis encompassing ADMET

* Corresponding author.

** Corresponding author.

E-mail addresses: Shopnil.ph@gmail.com (S. Akash), ib57001@student.gaziantep.edu.tr (I. Bayıl), sajjat.mahmood@gmail.com (S. Mahmood), nabendu21@rkmvccraahara.org (N. Mukerjee), amannahasan7890@gmail.com (T.A. Mili), dhama@rediffmail.com (K. Dhama), anisurrahmaniupharm@gmail.com (M.A. Rahman), swastikamaitra2018@gmail.com (S. Maitra), mmohany@ksu.edu.sa (M. Mohany), rejaie@ksu.edu.sa (S.S. Al-Rejaie), nalii@ksu.edu.sa (N. Ali), semwal.prabhakar@gmail.com (P. Semwal), rohitsharma@bhu.ac.in (R. Sharma).

<https://doi.org/10.1016/j.heliyon.2023.e20670>

Received 3 April 2023; Received in revised form 9 September 2023; Accepted 4 October 2023

Available online 5 October 2023

2405-8440/© 2023 Published by Elsevier Ltd.

This is an open access article under the CC BY-NC-ND license

(<http://creativecommons.org/licenses/by-nc-nd/4.0/>).

profiling, drug-likeness evaluation, principal component analysis (PCA), and molecular dynamic simulations (MDs) in comparison with the conventional drug, Mitomycin.

Results: The natural compounds investigated demonstrated superior docking affinities to *H. pylori* targets compared to the standard Mitomycin. Notably, the phytochemicals Diosgenin and Sarsapogenin stood out due to their exceptional binding affinities and pharmacokinetic properties, including favorable ADMET profiles.

Conclusion: Our comprehensive and technologically-advanced approach showcases the potential of identified phytochemicals as pioneering therapeutic agents against *H. pylori*-induced gastric malignancies. In light of our promising *in silico* results, we recommend these natural compounds as potential candidates for advancing *H. pylori*-targeted drug development. Given their potential, we strongly advocate for subsequent *in vitro* and *in vivo* studies to validate their therapeutic efficacy against this formidable gastrointestinal bacterium.

1. Introduction

Helicobacter pylori, a Gram-negative bacterium, exclusively colonizes the gastric mucosa and plays a significant role in peptic ulcer disease, gastritis, and gastric cancer [1]. It is affecting nearly 50 % of the global population [2], this persistent infection leads to chronic inflammation and an increased risk of duodenal and gastric ulcer diseases, as well as stomach cancer, the second most significant cause of cancer deaths worldwide [3]. *H. pylori*'s unique spiral shape and 3 to 5 polar flagella enable long-term survival in the stomach's highly acidic environment [4]. Gastric and esophageal cancers, known as gastric cancer (GC) and gastro-esophageal adenocarcinoma (GEA), are the fourth leading cause of cancer-related deaths [5]. The incidence of these diseases varies geographically, with the highest rates in Asia/Pacific and the lowest in America [6,7]. Treatment options for gastric cancer remain limited and often expensive, with many side effects [8]. Current therapies include chemotherapy, surgery, radiation therapy, hormonal therapy, antibiotics and immunotherapy [9]. *H. pylori* infection is the primary cause of precancerous lesions, leading to atrophic gastritis and intestinal metaplasia [10,11]. The bacterium's impact on gastric cell stress-adaptive pathways contributes to chronic infection and gastric disease development [12]. The onset of gastroduodenal disease due to *H. pylori* is linked to increased production of interleukin 8 and tumor necrosis factor-alpha (TNF-alpha) in the stomach [13]. Novel medications are urgently needed to reduce the global burden of gastric cancer incidents.

Several researchers have reviewed the anticancer potentials of natural sources, food products, and phytochemicals and their role in developing drugs and functional foods for the prevention and management of cancerous conditions, gastric cancer, countering *H. pylori* infection, and induced GC through mechanisms of action are yet to be elucidated completely and understood in a better way [14–20]. Traditionally, nature has been regarded as a highly effective source of medicine with minimal harmful side effects. It is widely believed that all possible remedies might be possible to obtain from natural sources [21,22]. Besides, natural products have been utilized throughout history, particularly in folk medicine to treat various ailments and diseases. This practice dates back to ancient times. The approaches of natural product chemistry have been around for a long time, allowing it to find a massive variety of bioactive secondary metabolites from terrestrial and marine sources. A significant number of these naturally occurring substances are now being considered for use as potential therapeutics. In Fig. 1, it is illustrated the development of Gastric cancer and the proposed mechanism action of our reported ligands.

This research highlights the remarkable potential of bioactive natural compounds in expediting the discovery of novel stomach cancer treatments. Computational study allows for a more efficient drug development process by reducing time, resources, and costs. Early identification of promising biomolecules helps minimize potential failures during wet lab experiment, paving the way for practical applications in designing and developing effective therapeutic option for the treatment of gastric cancer therapies [23].

2. Ligand selection and their earlier effectiveness of the studied compound

2.1. Glabridin

Glabridin, a prenylated isoflavone found in the roots of *G. glabra* L. (European licorice, Fabaceae), has a wide variety of biological effects, including antioxidant, anti-inflammatory, anti-atherogenic, regulation of energy metabolism, estrogenic, neuroprotective, anti-osteoporotic, and skin-whitening effects [24]. Glabridin has many biological functions and therapeutic benefits in cancer treatment [25], including anti-inflammatory and antioxidant properties. The pharmacological effects of Glabridin are numerous and include the prevention of *Staphylococcus*, *Candida*, and other bacterial infections, the treatment of metabolic abnormalities to reduce obesity, diabetes, and cardiovascular disease, the protection of nervous system function, the prevention of cancer, the treatment of inflammation, the treatment of osteoporosis, etc. Glabridin also acts as an estrogen substitute and has anticancer and anti-inflammatory properties [26].

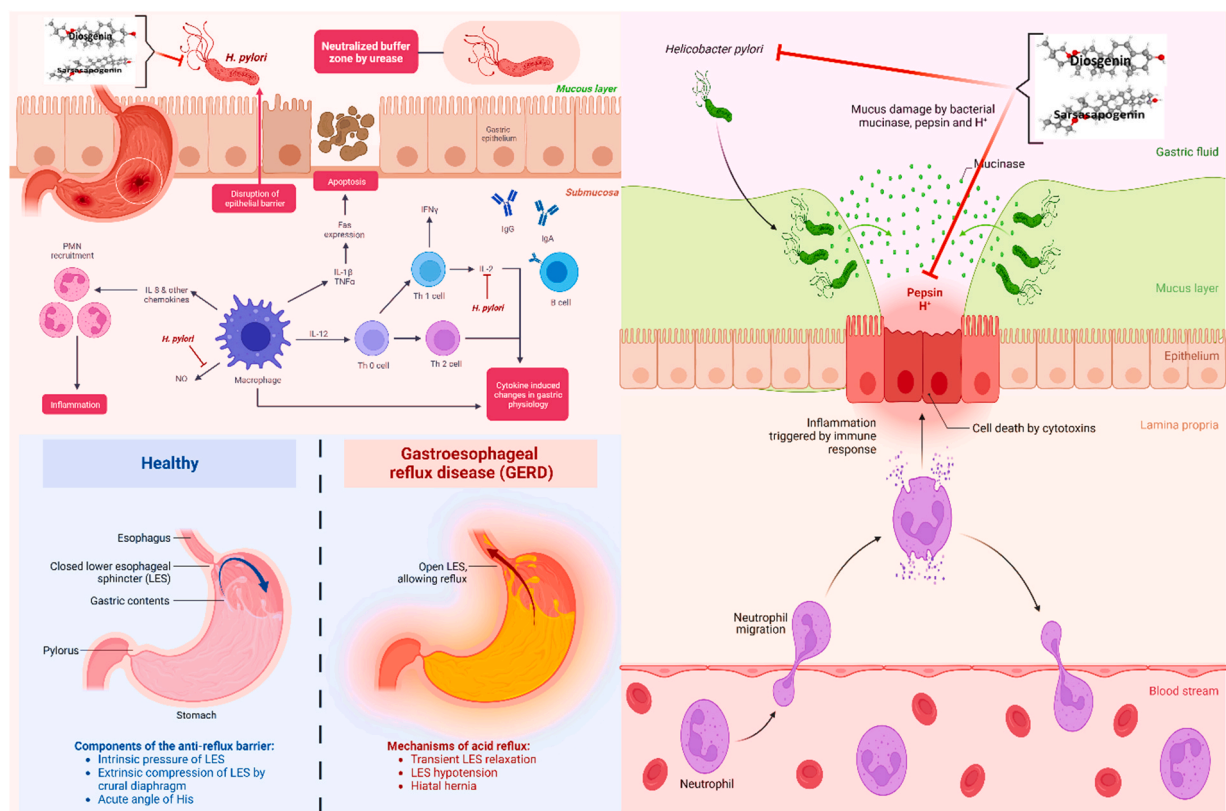


Fig. 1. Mechanism of action of proposed ligands against *H. pylori*, and inhibition of Gastric Cancer.

3. 2. Isoliquiritin

Isoliquiritin (ILQ) is one of the active elements of the traditional Chinese medicinal plant *Glycyrrhiza uralensis*, which has been used for hundreds of years to treat detoxification, swelling, and injuries as a herbal medicine [27]. *In vitro*, invasion and angiogenesis of cancer cells and endothelial cells are suppressed by isoliquiritin [28]. One of the extracts used in traditional Chinese medicine, isoliquiritin, has demonstrated an inhibitory impact on several malignancies, including stomach cancer and oral carcinoma [29].

3.1. Sanguinarine

Sanguinarine, a bioactive benzophenanthridine alkaloid, is found in plants of the *Papaveraceae* family and is used in traditional medicine [30]. Both the growth and invasion of gastric cancer cells are slowed by sanguinarine. The inhibitory efficacy of sanguinarine on Gastric Cancer cell proliferation was investigated by the CCK-8 test. Hence, we discovered that sanguinarine inhibited the expansion of GC cells while having minimal impact on GES-1 cells [31]. Inhibition of BGC-823 gastric cancer cell proliferation by sanguinarine is mediated through the downregulation of miR-96-5p/miR-29c-3p and the MAPK/JNK signaling pathway [22]. Furthermore, By modulating the TOX/DNA-PKcs/KU70/80 pathway, sanguinarine suppresses the growth of gastric cancer tumors [32].

3.2. Liquiritin

Licorice is regarded as a medicinal plant in China, Korea, and Japan and has several pharmacological properties, including anti-bacterial, anti-inflammatory, antioxidant, and even anticancer properties. The licorice flavonoid Liquiritin has been proposed to have anti-inflammatory and anticancer properties [33,34]. Liquiritin may inhibit the growth of human gastric cancer cells by inducing apoptosis. Apoptosis and autophagy are induced by liquidity through the miR-206/PI3K/AKT pathway in gastric cancer cells [33].

3.3. Glycyrrhetic acid

The bioactive component glycyrrhizin, found in high concentrations in licorice root, is rapidly converted by gut commensal bacteria into 18- β Glycyrrhetic acid [35]. Glycyrrhetic acid has anti-inflammatory, antioxidant, and cancer-preventive properties [36]. The viability of gastric cancer cells is significantly reduced by GA and 11-DOGGA in a dose- and time-dependent manner. Gastric

cancer cells treated with Glycyrrhetic acid undergo apoptosis and G2 phase arrest due to the overexpression of p21 and the downregulation of cdc2 and cyclin B1 [37].

3.4. Beta-carotene

Beta-carotene is a plant pigment in red, orange, or yellow foods. When the human body needs more vitamin A, it changes beta-carotene into vitamin A. Beta-carotene is a powerful antioxidant that prevents the damage that superoxide radicals can do to cells [38]. In humans, the beta-carotene (provitamin A) found in sea buckthorn benefits embryonic growth, a healthy pregnancy, and overall growth and well-being [39]. Beta-carotene ameliorates oxidative stress in lead-exposed workers by boosting glutathione metabolism and altering antioxidant defense mechanisms [40]. The combination of beta-carotene and vitamin A may help lower the risk of lung cancer in high-risk populations by acting as antioxidants [41].

3.5. Diosgenin

Diosgenin is a steroidal sapogenin found in high concentrations in various plants, including *Smilax China*, and *Trigonella foenum-graecum*. This compound has shown great promise and interest in treating a wide range of conditions, including cancer, hypercholesterolemia, inflammation, and several different types of infection [42]. Diosgenin has widespread *in vitro* anti-proliferative and pro-apoptotic actions on cancer cells [43]. Many studies have suggested Diosgenin may have potent anticancer properties [36]. Gastric cancer cells with hypoxia mimic-induced increased invasion and survival may be vulnerable to Diosgenin's anti-invasion and anti-proliferation effects [44]. Diosgenin has been shown to suppress the development of various malignancies. This includes breast, esophageal, liver, and stomach cancers. Diosgenin triggered autophagy and apoptosis in a human prostate cancer cell line [45].

3.6. Sarsasapogenin

The bioactive lead compound sarsasapogenin, found in *Anemarrhena asphodeloides* Bunge, has great promise in treating Alzheimer's disease [46]. Several pharmacological effects of Sarsasapogenin, including its anti-inflammatory, neuroprotective, and age-related memory impairment ameliorating properties, have been described [47]. Its altered structure and a number of its discovered derivatives have been shown to exhibit biological effects, including antitumor activity, antidepressant activity, anxiolytic-like action, and an A-reducing effect [48]. Sarsasapogenin is also effective against several cancers, including hepatocellular carcinoma and cervical carcinoma [49].

4. Materials and methodology

4.1. Determination of Lipinski rule and pharmacokinetics

Lipinski's rule and drug-likeness properties by Chris Lipinski analysis is a well-established approach to discriminate between molecules that resemble drugs and those proposed by Chris Lipinski [50,51]. The molecular weight of any drug molecule must be 500 g/mol or less. The lipophilicity value of drug molecules should not be more than 5 (calculated in logP unit), Any pharmacological molecule may have up to five hydrogen bond (H-bond) donors, but not more. Any drug molecule must only have no more than ten H-bond acceptors present in its chemical structure. According to Lipinski, any drug molecule following this rule should have a good oral drug candidate. Prediction of drug likeliness can immensely help medicinal chemistry develop more effective novel therapeutic compounds. To determine and analyze the drug likeliness and forecast of the data of Lipinski's five rules, the SwissADME online web server [52] (<http://www.swissadme.ch/index.php>) have been used and noted different parameters such as H-bond acceptor and donor, topological polar surface area (TPSA), molecular weight, number of rotatable bonds and Consensus Log P_{o/w} [53,54]. TPSA is a crucial factor in evaluating drug transport ability. Having a suitable TPSA value (<130 Å) indicates successful transportation of drug molecules, and the ideal TPSA value range is 20–130 Å [55,56]. Analysis of all these values will support electing the most appropriate compounds for the next steps.

4.2. ADMET analysis

If a molecule can be transported to its intended location with adequate concentration or quantity and must remain in the body for the anticipated time to execute a biological reaction, it may be regarded as a drug. For assessing these features, ADMET calculations were investigated. ADMET stands for absorption, distribution, metabolism, excretion, and toxicity. Calculating ADMET properties for any drug-like compound is crucial since around 50 % of drugs fail to violate these pharmacokinetics properties [57]. For that reason, successful ADMET for the selected compounds was calculated using a web-based tool called pkCSM (<https://biosig.lab.uq.edu.au/pkcsm/prediction>) [58]. The canonical SMILES of all molecules was collected from the PubChem database. Then those canonical SMILES were imported into the pkCSM server for ADMET data calculation. Our study prioritized ADMET properties like water solubility, Plasma Protein Binding, Human Intestinal Absorption, Caco-2 Permeability, Blood-Brain Barrier, Renal Organic Cation Transporter, CYP450 2C9, Hepatotoxicity, AMES toxicity, etc. ADMET properties of selected molecules were further compared with the standard drug's (Mitomycin) ADMET property.

4.3. Ligand preparation and molecular optimization

The main aim of this step is to assess various binding poses of interaction for identifying the most substantial interacting protein-ligand complex using an appropriate optimization method. This optimization method is immensely crucial because the precision of docking positively correlates with the procedure's effectiveness [59]. We have utilized Density functional theory (DFT) to rearrange atomic elements and optimize the geometry of the molecules so that we can achieve configuration with the minimum ground-state energy. All ligand structures were imported into the material studio program for utilizing the computational quantum mechanical modeling procedure density-functional theory (DFT) was applied [60]. Fig. 2 has displayed the 3D structure.

4.4. Target structure selection, preparation, and molecular docking study and visualization

The RCSB protein data bank was employed to obtain the three-dimensional (3D) structure of the proteins from *H. pylori* in PDB format [61]. The proteins of our interest are *H. pylori* -carcinogenic TNF-alpha-inducing protein (PDB ID: 3GUQ; Resolution: 2.47 Å Method: X-ray diffraction; Organism: *H. pylori*) and Crystal structure of protein Lpp20 (HP1456) from *Helicobacter pylori* (PDB ID:5OK8; Resolution: 1.87 Å; Method: X-ray diffraction; Organism: *H. pylori*) [62,63]. To prepare these proteins for molecular docking, the crystal structures were first cleaned using BIOVIA Discovery Studio Visualizer, such as missing hydrogen, incorrect bond order, and side-chain shape, which has been corrected along with removing the excess molecules such as water and unwanted hetero atoms to get a purified protein structure for molecular docking [64]. In most cases, water molecules do not contribute to the substrate or drug's binding with the receptor. Hence, they were eliminated to simplify computations and relieve the binding location. Besides, previously docked unwanted hetero atoms can occupy the receptor's desired active site. As a result, they were removed to free up the active site allowing calculations to be carried out more quickly. Molecular docking was performed using PyRx software packages [65]. Swiss-Prot

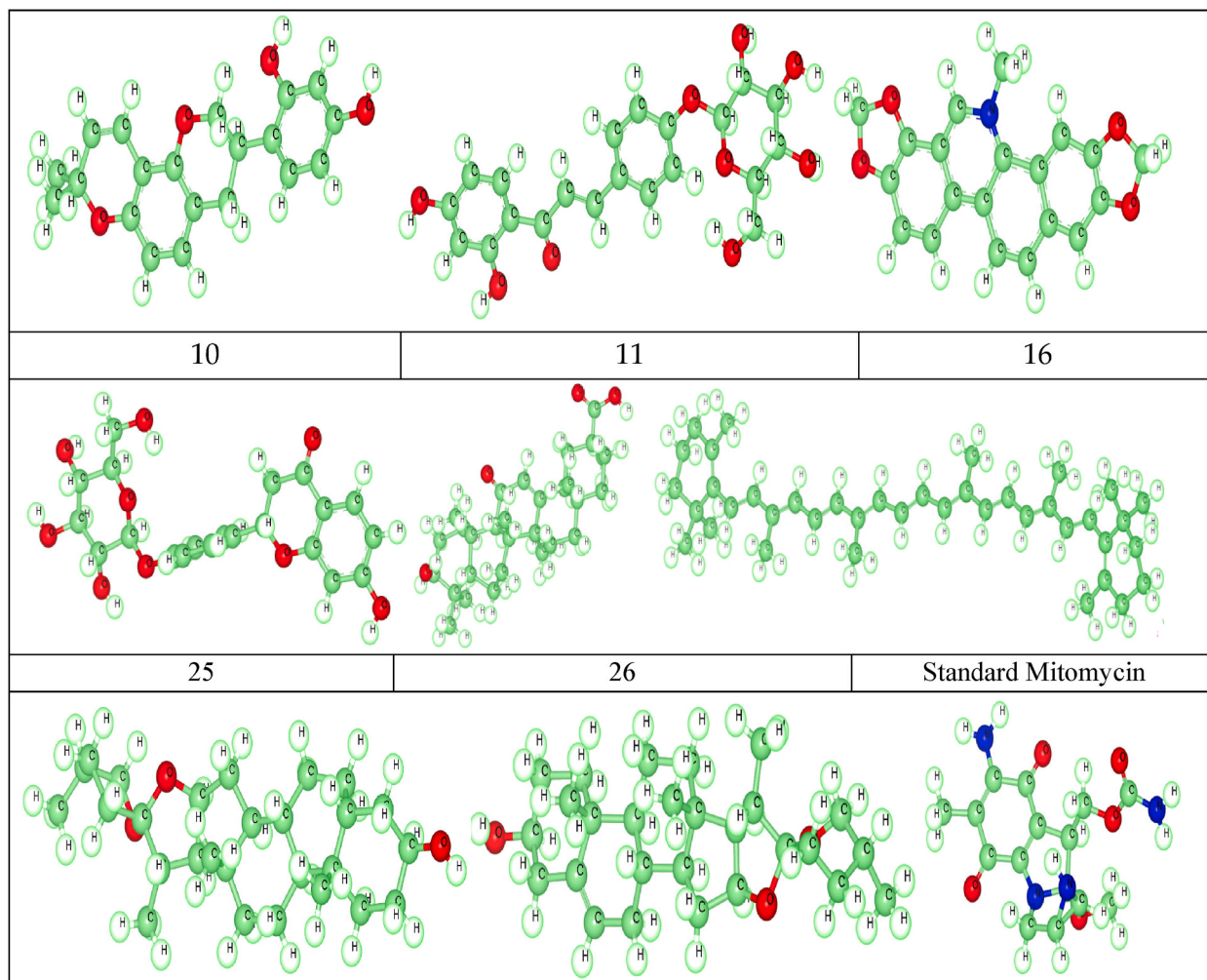


Fig. 2. The three-dimensional (3D) structures of the most suitable eight molecules and the standard molecule.

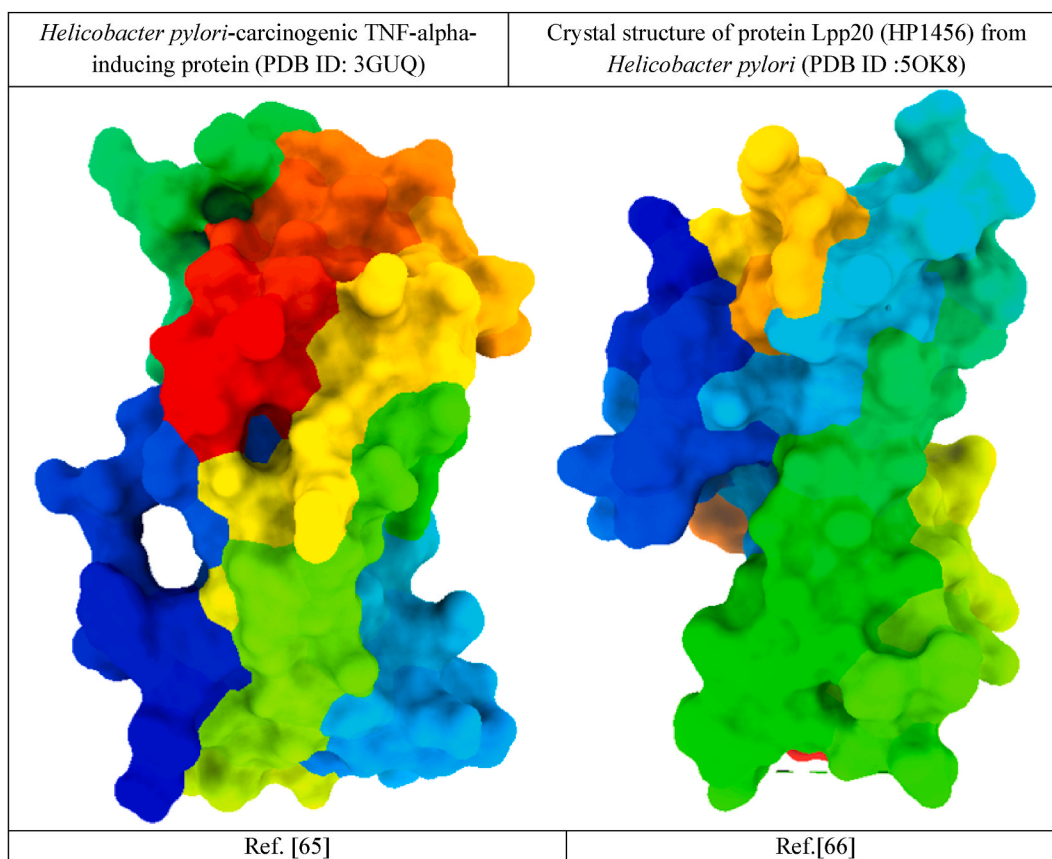


Fig. 3. Three-dimensional protein structure of the targeted protein.

database browser (Swiss PDB Viewer) was used to reduce the energy of the target protein prior to molecular docking [66]. The purified protein structures were imported in PDB format, and ligand structures were imported in pdbqt format. The grid center points were set to X = -31.68, Y = -17.18, Z = 25.1838, and the box dimensions (Å) X = 37.31, Y = 55.63, Z = 44.96 for (PDB-ID: 3GUQ), and the grid center for (PDB ID 5OK8); X = -8.7259, Y = -31.6119, Z = -27.5813, and box dimension X = 81.3565, Y = 55.5874 and Z = 91.9504 were set so that the grid box could wrap the whole substrate binding pocket of the protein structure. The three-dimensional structures of the proteins are represented below in Fig. 3.

4.5. Molecular dynamic simulations (MD) methods

MD simulations are essential to proving the stability of proteins because they give precise information on fluctuations and conformational changes in protein-ligand complexes as they approach their stable state. As a result, MD simulation was utilized in this study to understand better the stability of protein binding complexes involving the diosgenin-protein complex, the sarsasapogenin-protein complex, and the standard mitomycin-protein complex. As a starting point for simulation, the docked structures of the proteins Diosgenin, Sarsasapogenin, and standard Mitomycin with a ligand were used. The CHARMM36 force field and the Gromacs version 2020 software package were utilized in the simulations run for 100 ns within a periodic water box. The CHARMM-GUI server produced the force field for the ligands and the proteins [67,68]. The complexes were placed inside a rectangular box with a buffer distance of 10 in each direction. The box was then solvated with water molecules that were composed of TIP3P. Adding 36 Na⁺ ions and 36 Cl⁻ ions neutralized the system's charge for the Diosgenin ligand, Sarsasapogenin ligand, and standard Mitomycin ligand. After that, 0.015 M of NaCl was added to make an environment similar to the cells in terms of how it worked. Structure minimization of the docked complexes was performed using a charmm36 forcefield. Each of the whole systems was equilibrated at 310 K temperature, each for 5000 steps (i.e., 10 PS). The NPT ensemble's production run lasted 100 s. Hydrogen was constrained using the Lincs technique; hence, the timestep was set to 2 fs. A switching method of 12–14 was utilized to determine all of the van der Waals forces, and the cutoff value was determined to be 14. The particle mesh Ewald (PME) approach, with a maximum grid spacing of 1.2, was used to calculate long-range electrostatic interactions. The PME computations were conducted at each step; there was no use of a multiple-time stepping scheme. The temperature was held at 310 K. The target for the system size changes in the barostat was set to 1 bar. The time step for integrating was 2 fs. After beginning by re-centering, the simulation output, the trajectories were evaluated using the VMD (University of Illinois at Urbana-Champaign, Urbana, IL, USA) program, Bio3D, and QTGRACE, respectively. Several analysis approaches were utilized for

trajectory analysis, such as RMSD and RMSF calculations, the development of the radius of gyration, the number of H-bonds, and principal component analysis (PCA) [69].

4.6. Binding free energy calculation using MM-PBSA

The molecular mechanics Poisson-Boltzmann surface area (MMPBSA) is vital when evaluating the biophysical basis for proteins and their binding to ligands, which are Diosgenin, Sarsasapogenin, and standard Mitomycin. MM-PBSA calculation was carried out to examine the binding free energy of protein-ligand complexes. Binding free energy (ΔG) estimation was done by eq. (3) using the script MMPBSA.py of the AMBER package [70]. The single trajectory protocol approach was used for MM-PBSA calculation, which involved only the simulation of the protein-ligand complex forms. Using the binding free energy of a protein-ligand complex is estimated as follows [71]:

$$\Delta G = \langle GPL \rangle - \langle GP \rangle - \langle GL \rangle \quad \text{eq. X}$$

Where ΔG_{bind} denotes the binding free energy, GPL is the free energy of the protein-ligand complex, GP is the free energy protein, GL is the free energy of the ligand, and $\langle \rangle$ represents the ensemble average.

Equation X can be approximately written as

$$\Delta G = \Delta E_{\text{MM}} + \Delta G_{\text{SOLV}} - T\Delta S \quad \text{eq. Y}$$

where ΔE_{MM} denotes the molecular mechanics' gas-phase interaction energy change upon ligand binding and ΔG_{SOLV} , $T\Delta S$ represents the solvation-free energy change, and $T\Delta S$ is the entropic contribution to ΔG at absolute temperature T. MM-PBSA method calculates the ΔE_{MM} part using molecular mechanics force field, polar region of the solvation free energy with linearized Poisson Boltzmann model and a polar part using surface area approach [72].

5. Results & analysis

5.1. Lipinski rule and drug-likeness

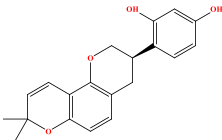
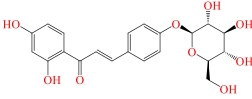
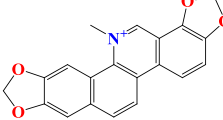
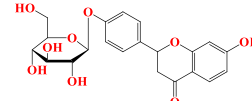
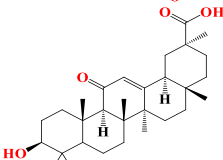
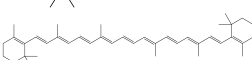
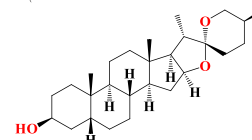
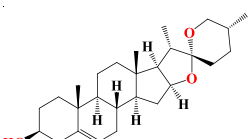
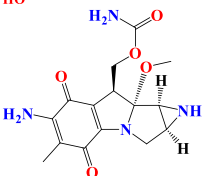
The Lipinski rule and drug-likeness profiling are effective ways to identify drug-like molecules, as many drugs fail in the initial evaluation phase for lacking suitable drug-like properties. The physicochemical properties of selected compounds and Mitomycin (standard compound) predicted using SwissADME are represented in Table 1. Lipinski's rule states that any drug-like compound's molecular weight should not exceed 500 g/Mol. In our current study, all the compounds have a molecular weight of less than 500g/Mol, making them suitable for drug-like behavior. In addition, no drug-like compounds should have more than 5 H-bond donors, as stated in the Lipinski rule. All the selected compounds had less than five H-bond donors except Isoliquiritin, which violated this feature by containing six H-bond donors in its chemical structure.

In the same way, the total number of H-bond acceptor were also calculated, where any drug-like molecule was supposed to have a maximum of 10 H-bond acceptors. By assessing the data from Table 1, we can confirm that all the compounds contained less than ten H-bond acceptors. The consensus log Po/w was used to calculate the mean anticipated lipophilicity values, which were used to determine the compound's non-aqueous solubility, also presented in Table 1. This means that a molecule's consensus log Po/w values will be more negative if it is more soluble. TPSA data revealed that all the compounds had a TPSA value $<130 \text{ \AA}^2$ except Isoliquiritin and Liquiritin. The highest TPSA value obtained from our selected compounds was 156.91 \AA^2 (Isoliquiritin), and the lowest TPSA value expressed was 38.69 \AA^2 (Diosgenin and Sarsasapogenin). The ideal TPSA score of Glabridin, Sanguinarine, Glycyrrhetic acid, Beta-carotin, Diosgenin, and Sarsasapogenin indicates that the majority of our selected compounds contain the vital ability of drug transport. Eventually, all eight proposed compounds successfully followed Lipinski's rule of five, as none of these compounds had more than one rule violation, whereas Glabridin, Liquiritin, and Sanguinarine had zero violations. The Lipinski Rule has played an essential role to establish a potential drug in computational drug design. It guides newly developed bioactive molecules to provide the chance of

Table 1
Theoretical data of Lipinski rule predicted by SwissADME.

S/ N	Ligand Name	Molecular weight	Number of rotatable bonds	Hydrogen bond acceptor	Hydrogen bond donor	Topological polar surface area \AA^2	Consensus Log $P_{o/w}$	Lipinski rule	
								Result	violation
04	Glabridin	324.37	1	4	2	58.92	3.45	Yes	0
05	Isoliquiritin	418.39	6	9	6	156.91	0.2	Yes	1
07	Sanguinarine	332.33	0	4	0	40.8	2.88	Yes	0
10	Liquiritin	418.39	4	9	5	145.91	0.25	Yes	0
11	Glycyrrhetic acid	470.68	1	4	2	74.6	5.17	Yes	1
16	Beta-carotin	470.77	28	4	2	66.76	8.32	Yes	1
25	Sarsasapogenin	416.64	0	3	1	38.69	5.24	Yes	1
26	Diosgenin	414.62	0	3	1	38.69	5.02	Yes	1
	Standard Mitomycin	334.33	4	6	3	146.89	-0.8	Yes	0

Table 2
Binding Affinity against *Bacteria Responsible for stomach cancer*.

S/ N	Name	Chemical structure	Lpp20 (HP1456) from <i>H. pylori</i> (PDB ID:5OK8)	<i>H. pylori</i> -carcinogenic TNF-alpha-inducing protein (PDB ID 3GUQ)
			Binding Affinity (kcal/mol)	Binding Affinity (kcal/mol)
04	Glabridin		-8.3	-8.2
05	Isoliquiritin		-8.0	-7.9
07	Sanguinarine		-9.2	-8.7
10	Liquiritin		-8.1	-8.1
11	Glycyrrhetic acid		-8.0	-8.7
16	Beta-carotin		-8.4	-8.0
25	Sarsasapogenin		-8.3	-9.1
26	Diosgenin		-9.1	-9.4
	Standard Mitomycin		-6.3	-7.0

drug-like properties and able to minimize the number of molecules which may chance to fail in preclinical and clinical studies due to drug-like properties, which ultimately helps to reduce the cost, and resources and improve the efficiency of drug [73,74].

5.2. Molecular docking analysis against targeted receptor responsible for gastric cancer

Initially, thirty natural compounds are were prepared for molecular docking (Supplementary Table S1) and based on maximum affinities, eight topmost compounds were selected to conduct further studies against two target bacterial proteins responsible for gastric cancer, including *H. pylori*-carcinogenic TNF-alpha-inducing protein and crystal structure protein Lpp20 (HP1456). One of the key tools in computer-aided drug design is molecular docking. Which is utilized for binding affinity, non-bond interaction, finding docking pockets, and making protein-ligand complexes. Hydrogen and hydrophobic bonds in protein-ligand complexes play a crucial role in the docking score, and -6.00 kcal/mol or above is considered the standard docking score for AutoDock [75]. Here all reported

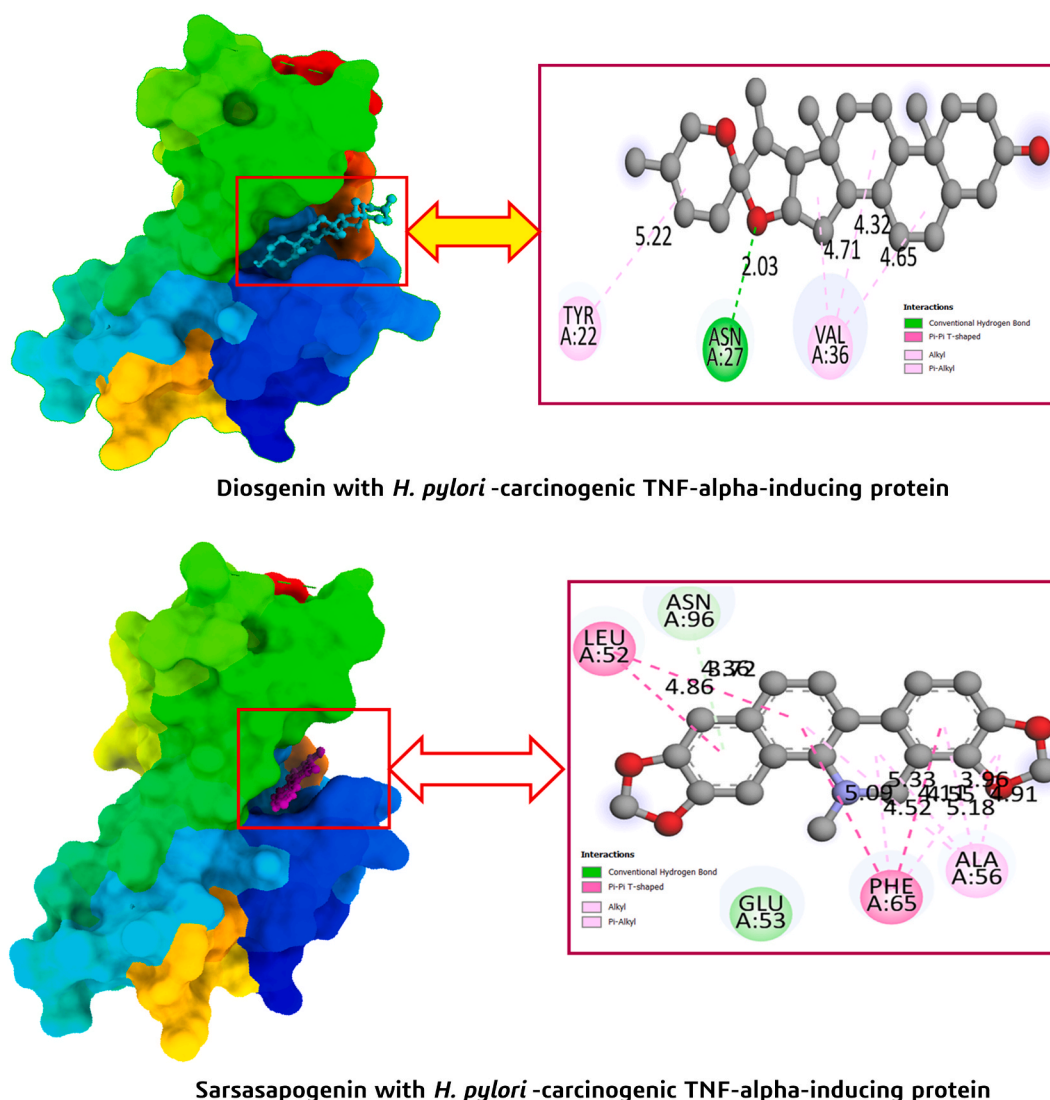
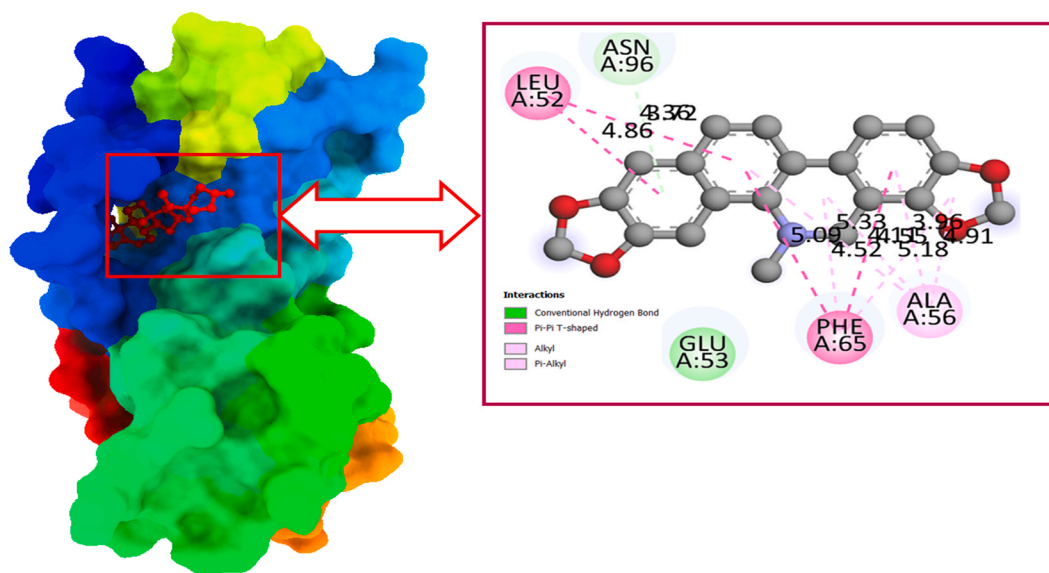


Fig. 4. Docking interactions between the proposed compound and target protein.

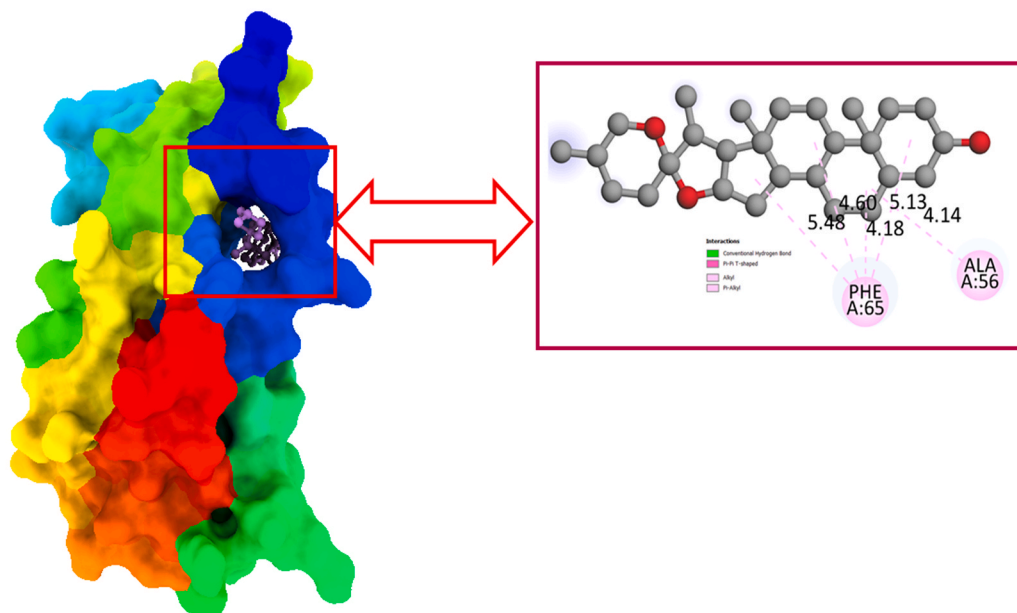
compound has better binding affinity and greater than -6.00 kcal/mol. More specifically, the binding affinity with *H. pylori*-carcinogenic TNF-alpha-inducing protein range from -7.9 kcal/mol to -9.4 kcal/mol, and with crystal structure protein Lpp20 (HP1456) from -7.2 kcal/mol to -9.2 kcal/mol where highest binding affinity with two target macromolecule is -9.4 kcal/mol and -9.2 kcal/mol respectively. Controlled drug Mitomycin has lowest binding affinity than our reported ligand, which is -7.0 kcal/mol with *H. pylori*-carcinogenic TNF-alpha-inducing protein and -6.3 kcal/mol with protein Lpp20 (HP1456) from *H. pylori*. So, the reported compounds could be more effective and inhibit the targeted receptor for treating gastric cancer. In Table 2, the reported binding affinities have been listed.

5.3. Molecular docking pose and interaction analysis

Protein-ligand interaction is essential in discovering new drugs, which provides information about binding and bonding drug molecules with target pathogenic proteins [76]. This interaction is necessary to determine the therapeutic goal. The interaction between *H. pylori*-carcinogenic TNF-alpha-inducing protein and Lpp20 (HP1456) protein has been investigated with bond distance. According to Table 2, Diosgenin and Sarsasapogenin have the highest binding affinity with *H. pylori*-carcinogenic TNF-alpha-inducing Protein in Fig. 3 represents their docking pocket and ligand-protein interactions. The binding residues are at ASN-27 (2.03) as conventional hydrogen bonds, and TYR-22 (5.22) and VAL-36 (4.71, 4.32, 4.65), three different interactions with the ligand are present as hydrophobic bonds with Diosgenin where Sarsasapogenin ligand makes four conventional hydrogen bonds with VAL-36 (3.24, 4.04, 4.24, 5.09) amino acid with the target protein.



Sanguinarine with Lpp20 (HP1456) protein from *H. pylori*



Diosgenin with Lpp20 (HP1456) protein from *H. pylori*

Fig. 4. (continued).

Furthermore, the docking pose and interaction of the Lpp20 (HP1456) protein from *H. pylori* with Diosgenin and sanguinarine are also represented in Fig. 4. Binding residues and bonds with sanguinarine and target proteins are conventional H-bonds with GLU-53 and ASN-96 amino acids, whereas LEU-52, PHE-65, and ALA-56 are formed hydrophobic interactions, —five hydrophobic bonds with Diosgenin, four with PHE-65, and one with ALA-56 amino acid.

5.4. MD simulation results

MD simulation studies were conducted in addition to the above-mentioned computational methods to identify the best interactions of Diosgenin, Sarsasapogenin, and standard Mitomycin protein binding complexes and to study their effectiveness and stability over time. The root-mean-square deviation (RMSD) of the protein backbone, complex structure, and ligand structure was examined to determine the stability of protein-ligand complexes during the simulation period. Furthermore, MD simulation trajectories were examined to determine various criteria, including the root-mean-square fluctuation (RMSF), the radius of gyration (Rg), H-bond

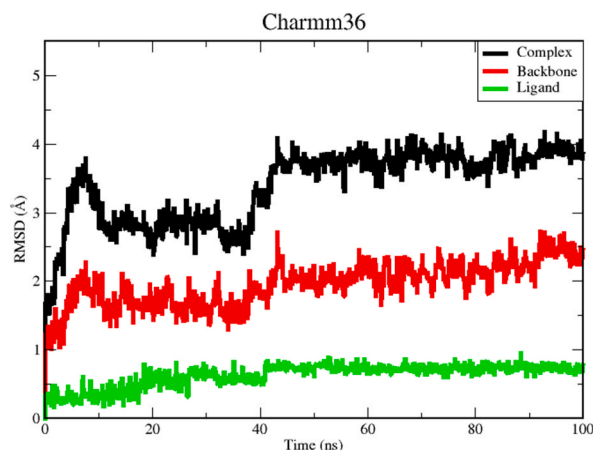


Fig. 5. The RMSD (root-mean-square deviation) between the Diosgenin and the complex protein backbone.

analysis, and principal component analysis (PCA). Here, a thorough description of each parameter's findings is provided. As illustrated in Fig. 5, the RMSD of the protein backbone, the Diosgenin complex, was computed during a 100 ns MD trajectory to evaluate the stability of each protein-ligand complex. RMSD is a fundamental method to analyze structural stability. Therefore, large RMSD values would be connected to a significant degree of conformational change within the molecule under investigation. When analyzing a protein-ligand complex, one of the most important parameters to consider is the root mean square deviation (RMSD) of the C α atoms in the protein backbone. This parameter describes the conformational stability of the complex as a whole while it is in a dynamic state and being simulated. As shown in Fig. 5, the RMSD plot of the backbone atom of the protein concerning its initial position significantly increased to 2.2 Å for the first 7 ns following its initial position, then slightly decreased and kept on stabilizing until 40 ns and substantially increased to 2.7 Å at 43 ns of the trajectory. After that, the backbone shows a decreasing trend from 2.7 Å to 2.3 Å, and from 45 to 95 ns, the backbone shows continued slight fluctuation. Fig. 5 shows that the average RMSD value of the protein backbone was 1.806 Å.

The RMSD was calculated using a 100 NS MD simulation. The RMSD of the protein backbone is depicted in red. The diosgenin complex of RMSD is depicted in black. The RMSD of the ligand is depicted in green. On the other hand, the RMSD plot in Fig. 6 for Sarsasapogenin with *H. pylori* showed that its initial position during the full MD simulation showed that it became dynamically stabilized for the first time around 50 ns. The significant abrupt change in RMSD values of the backbone protein is observed to be between 50 and 60 ns. After that time, the RMSD graph line shows a decrease from 2.8 Å to 1.5 Å and an increase of 2.1 around 63 ns. Then demonstrate a steady-state, stable graph line with slight fluctuation until the end of the simulation. Fig. 6 shows that the average RMSD value of the protein backbone was 1.370 Å.

The RMSD between the Sarsasapogenin and the complex protein backbone was calculated using a 100 NS MD simulation. The Sarsasapogenin complex RMSD is depicted in black. The RMSD of the ligand is depicted in green. The RMSD (root-mean-square deviation) between the standard Mitomycin complex and protein backbone was calculated at 100 NS MD simulations. The protein backbone average RMSD value was 1.386 Å for standard Mitomycin.

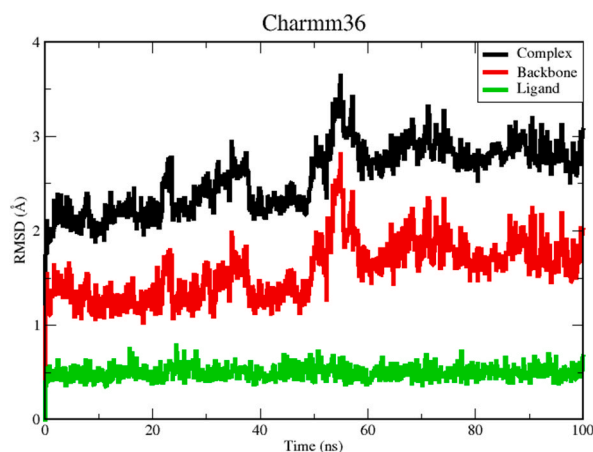


Fig. 6. RMSD (root-mean-square deviation) complex protein backbone.

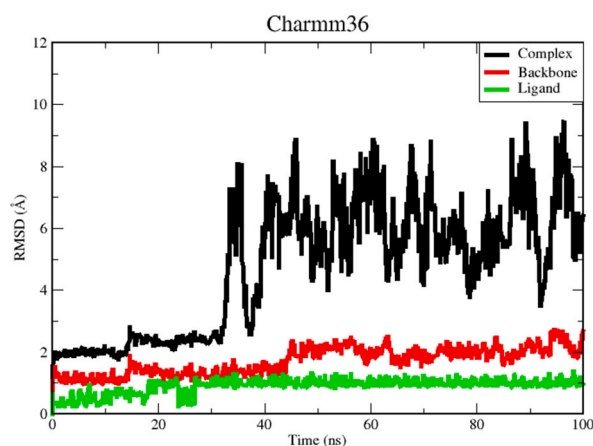


Fig. 7. The RMSD between the Standard Mitomycin and the complex protein backbone was calculated using a 100 NS MD simulation.

In the comparison of ligands RMSD in Figs. 5 and 7, the ligand average RMSD is 1.235 Å and 1.249 Å, respectively. But the average RMSD of ligands in Fig. 6 was 1.496 Å. The ligand in Fig. 6 showed a higher RMSD value compared to the RMSD of Figs. 5 and 6 simulations. However, Fig. 6 ligands indicated considerable stability of the complex with high RMSD values. When we analyzed the trajectories using VMD software, we observed that the Sarsasapogenin ligand did not jump out of the protein domain, which means this ligand was located inside the binding site. Therefore, from ligand RMSD analysis, it is clear that Sarsasapogenin's ligand-binding orientation has not changed over the simulation time. Both diosgenin and standard Mitomycin have changed their conformational orientation and deviated. This indicates that, in the case of diosgenin protein and standard protein, both ligands showed multiple binding orientations, and these ligands moved out of the binding pocket in MD simulations. It was determined that the docking poses were inappropriate for the candidate with a complex structure.

The RMSD of the protein backbone and the ligand were computed during the course of a 100 ns MD trajectory, as illustrated in Figs. 5, 6, and 7, to assess the stability of each protein-ligand combination. The complexes' average RMSD values were 3.981 Å, 2.925 Å, and 5.138 Å, respectively. Protein-ligand complexes in Fig. 6 were stable, whereas those in Figs. 7 and 5 were not, as measured by RMSDs. The RMSD value was less than 3.0 for the stable complexes, including Sarsasapogenin, whereas it was greater than 3.0 for the diosgenin complex. This suggests that the ligand-backbone connections established in the first simulation were preserved in the second. When complexed with diosgenin and standard Mitomycin after the simulation, the ligands appeared highly unstable. The ligands displayed significant fluctuations, demonstrating the complex's overall instability. However, the sarsasapogenin complex showed considerable stability.

The RMSF data of the protein backbone and complexes were plotted to visualize the average fluctuation of all the amino acid residues, which for a 100 ns MD trajectory is seen in Fig. 8. The protein residues are crucial in achieving a stable shape for a protein-ligand complex, which may be assessed using the RMSF parameter. The considerable RMSF value indicates greater flexibility, whereas the lesser RMSF values indicate a more stable zone. Thus, more RMSF displaying residues or groups suggest greater flexibility, suggesting a greater possibility for interaction with ligand molecules. Furthermore, lower RMSF fluctuations are associated with less flexibility, resulting in diminished interaction ability. In Fig. 8A, the fluctuations of significant peaks in the RMSF graph were observed with the backbone residue positions between ASP19–VAL20, LEU25–ARG28, VAL42–GLU48, LEU75–GLU88, ASN112–GLU116, SER140–GLN144, and LYS158–SER160. In Fig. 8, significant fluctuations were observed at regions from residue indexes 19–22, 26–28, 40–46, 80–89, 106, 114–117, and 158–161 (Fig. 8A).

For Fig. 8B, an RMSF graph was observed with the backbone residue positions between ASP19–GLN26, VAL42–GLU49, ASN79–GLU88, ASN112–GLU116, and LYS158–SER160. In Fig. 8, the complex, major fluctuations were observed at regions from residue indexes of 19–28, 40–49, 80–83, 110–114, 1281–30, 137–144, and 158–161 (Fig. 8B). For (Fig. 8C), in RMSF graph was observed with the backbone residue positions between ASN19–TYR22, VAL42–GLU49, ARG80–GLU88, PRO113–ASN115, HSD137–GLN144, and ASP159–SER160. In Fig. 8C, complex, significant fluctuations were observed at regions from residue indexes of 19–20, 25–30, 43–44, 80–84, 114–115, 143–144, and 161 (Fig. 8C). These indicate that In (Fig. 8B), the protein backbone and the complex have the lowest RMSF value, while in (Fig. 8A) and (Fig. 8C) have higher RMSF values. In comparison, the RMSF values were most prominent in the cases of Diosgenin and conventional Mitomycin; however, they were less prominent in the case of sarsasapogenin-bound protein, which indicates that the ligand binding gives higher stability to most of the areas of the protein.

The RMSF of the protein backbone is depicted in red. The complex's RMSF is depicted in black. Using the radius of gyration (Rg) to assess the structural integrity of the studied systems is an effective method of determining their compactness and structural integrity. This concept describes how far apart atoms are from their average mass as measured by their root mean square distance (RMSD).

This study uses Rg to assess changes in the compactness of ligand-protein complexes (shown in Fig. 9). In a complex protein, the mass of the atoms is measured about the center of mass using a parameter called the radius of gyration. standard Mitomycin-complex displayed an average Rg value of more than 1.81 Å and showed more deviation after 30 ns. Diosgenin-complex and sarsasapogenin-complex showed an average Rg value of 1.72 Å and 1.71 Å, respectively, and was not observe any deviation during the simulation

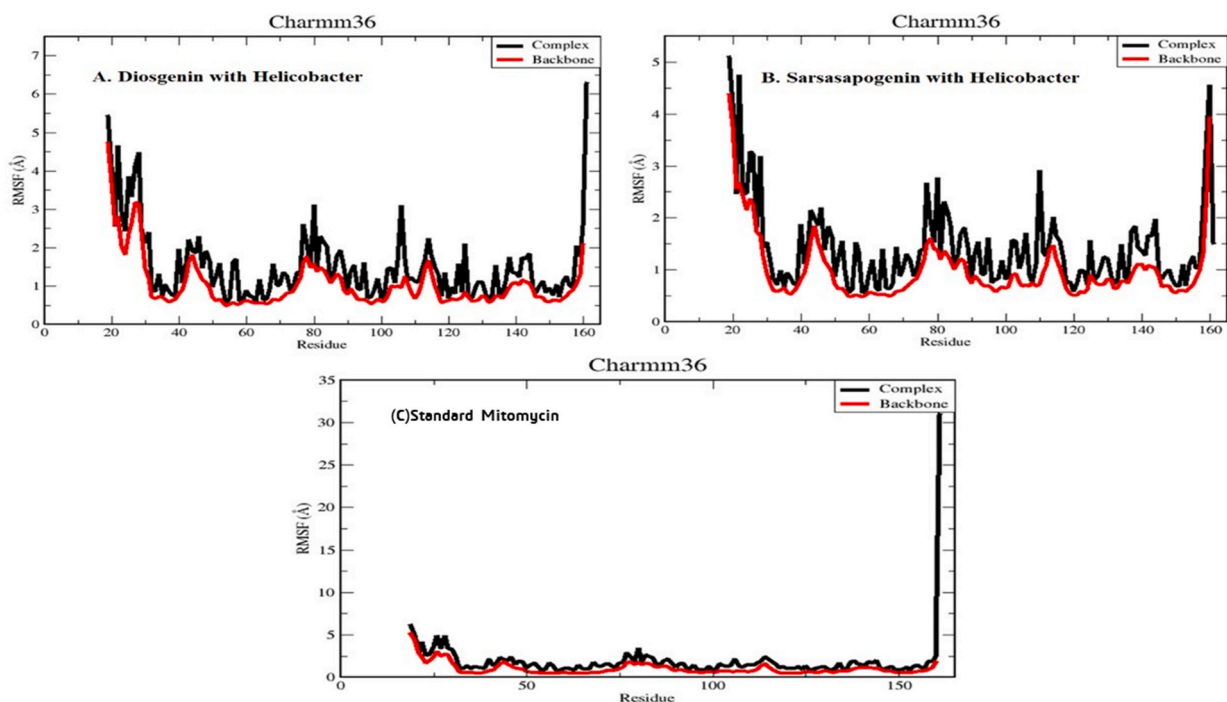


Fig. 8. Derived from a 100 ns MD simulation, the RMSF of a complicated protein backbone.

period of 100 ns. Both the protein complex's structural compactness and its overall compactness were distinct from one another. The Diosgenin-complex and the Sarsasapogenin-complex were found to have undergone no significant changes, and the complexes retained their stability and compactness. Despite this, fluctuations in its composition were reported for the standard Mitomycin complex, which suggests that the complex has lost some of its compactness.

The number of H-bonds formed by the ligand molecule with the proteins (Diosgenin, Sarsasapogenin, and standard Mitomycin) was calculated and plotted on a graph, and the results may be found in Fig. 10. Stabilizing protein-ligand complexes is dependent on the intermolecular H-bonding between the protein and ligand. The stability of the H-bond network formed between proteins (Diosgenin,

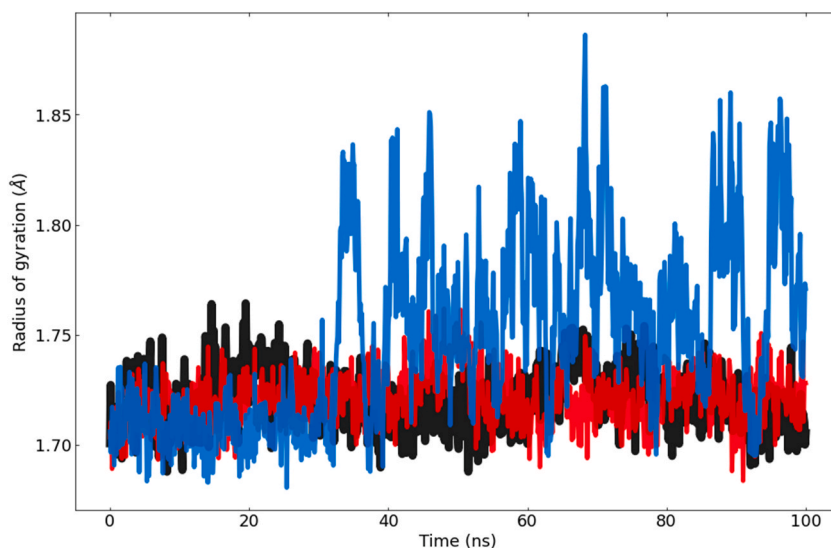


Fig. 9. From a 100-ns MD simulation, the radius of gyration (Rg) values of the diosgenin-complex, sarsasapogenin-complex, and standard mitomycin-complex. The Rg of the diosgenin complex is depicted in black. The RG of the sarsasapogenin complex is shown in red. The standard mitomycin-complex Rg is depicted in blue. (For interpretation of the references to color in this figure legend, the reader is referred to the Web version of this article.)

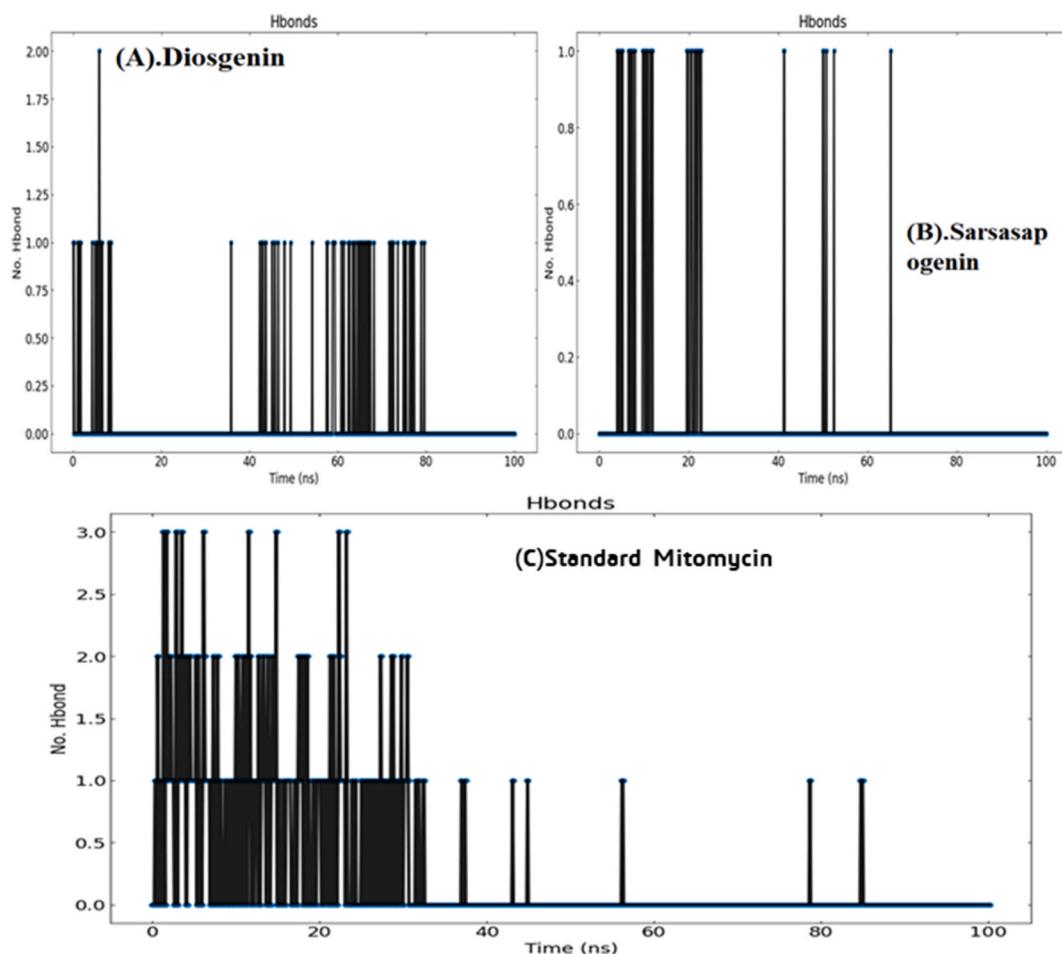


Fig. 10. After MD simulation for 100 ns, the number of H-bonds generated by the ligand's molecule was determined.

Table 3

H-bonds formed by the ligand molecule with the targeted proteins.

Donor	Acceptor	Occupancy
Diosgenin		
ASN27-Side-ND2	UNK0-Side-O1	0.60 %
Sarsasapogenin		
UNK0-Side-O3	GLN34-Side-OE1	4.99 %
GLN34-Side-NE2	UNK0-Side-O3	0.10 %
UNK0-Side-O3	TRP23-Main-O	0.10 %
Standard Mitomycin		
GLN34-Side-NE2	UNK0-Side-O3	0.10 %
GLN34-Side-NE2	UNK0-Side-O4	4.79 %
UNK0-Side-N4	TRP23-Main-O	0.80 %
UNK0-Side-N3	TRP23-Main-O	0.50 %
ASN65-Side-ND2	UNK0-Side-N1	0.60 %
UNK0-Side-N4	LEU25-Main-O	0.20 %
UNK0-Side-N3	LEU25-Main-O	0.30 %
VAL36-Main-N	UNK0-Side-O1	0.80 %
UNK0-Side-N3	VAL36-Main-O	1.40 %

Sarsasapogenin, and standard Mitomycin) and ligands have been calculated throughout the 100 ns simulation period. It was expected that the number of generated H-bonds would be a function of the simulation time to determine whether or not the system was stable while it was being simulated. Here, the hydrogen bond criteria were set as the distance of acceptor-donor < 0.30 nm and the angle > 120 . 0.30 nm is a common choice of H-bond distance in literature. The frames used for this calculation were collected at 2-ps intervals from the whole 100-ns MD trajectory. Hydrogen bonds contribute to bonding and are worthy of investigation due to their tenacity.

Table 4
Binding energy results.

	Δ EVDW (kJ/mol)	Δ EEEL (kJ/mol)	Δ GPB (kJ/mol)	Δ GNP (kJ/mol)	Δ GDISP (kJ/mol)	Δ G Binding (kJ/mol)
Diosgenin	-22.68	-0.96	8.74	-2.91	0.0	-17.81
Sarsasapogenin	-36.52	0.38	14.48	-4.28	0.0	-25.93
Standard Mitomycin	-0.71	-0.44	1.08	-0.20	0.0	-0.27

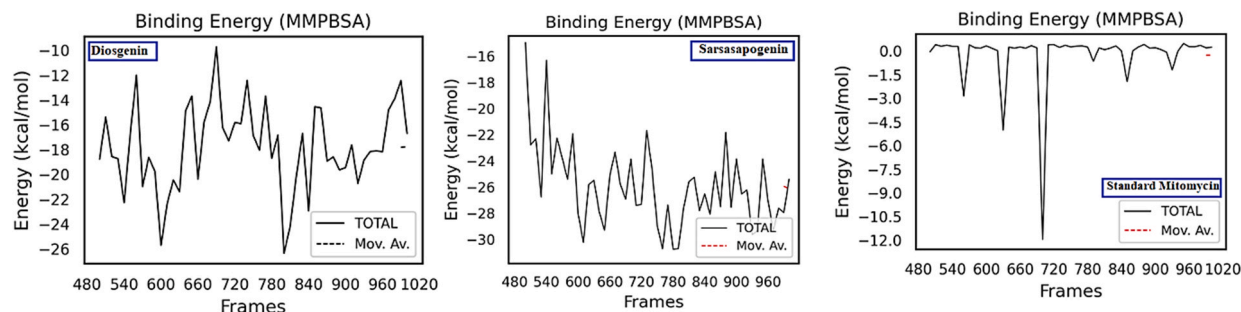


Fig. 11. Graphically displayed the binding free energy.

Using the VMD H-bonding analysis tool, all conceivable H-bonding interactions between the two specified areas, in this example, the protein and the ligand, have been explored throughout time. The result computes the total number of H-bonds and occupancy over time. These numbers can be acquired from the 'Percentage occupancy of the Hbond' output of the H-bond analysis tool. The 'Percentage occupancy of the H bond' output of the H-bond analysis tool provides these values. The docked complex forms a great deal more hydrogen bonds. Molecular Dynamics (MD) simulations showed that the H-bonds in docking structures were maintained; other H-bonds were also observed. Table 3 details the individual occupancy of detected H-bonds per ligand for Diosgenin, Sarsasapogenin, and standard Mitomycin.

A vital role hydrogen bonds play in detecting non-bonding interactions between proteins and ligands is their capacity to indicate non-bonding interactions. The H-bond occupancies at ASN27 with the ligand are 0.60 % (Table 3). Regarding the Diosgenin complex, during MD, the complex stability was maintained by interactions with ASN27 residue.

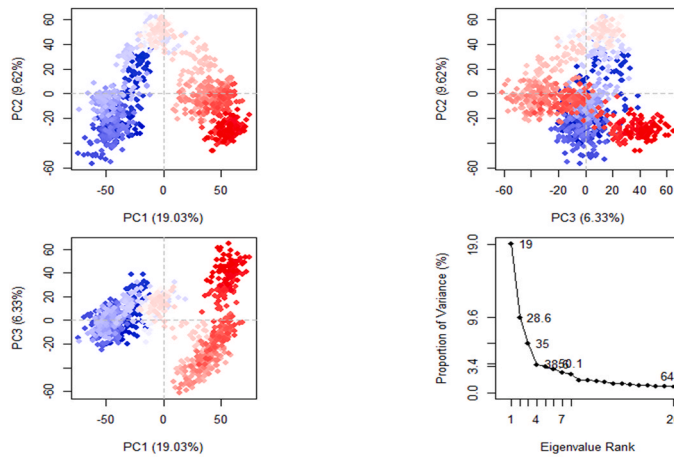
The compound Diosgenin formed only one H-bond found in docked simulation. Diosgenin with a complex exhibited fewer H-bonds throughout the simulation, indicating that most of them appeared first at ten ns, 40–60 ns, and primarily occurred at 60–80 ns. But for the sarsasapogenin complex, three H-bonds were observed. These H-bonds appeared first at 20 ns and 40–60 ns during the simulation time. The three H-bonds were not found in docked simulations. For the standard mitomycin complex, multiple H-bonds were identified. In the system, H-bonds were stable; most appeared between 0 ns and 40 ns. The compound formed forty-seven H-bonds, including nine new H-bonds that were not found in docked simulations. The compound interacted with GLN34 with two H-bonds of 2.02 Å, ASN65 with a 2.01 Å H-bond, two H-bonds of 1.93 Å length with TRP23, two H-bonds of 1.81 Å and 1.75 Å lengths with VAL36, and two H-bonds of 1.81 Å and 1.75 Å lengths with LEU25. The complex exhibited more H-bonds throughout the simulation time, indicating that the protein has stable and robust H-bonds with ligands.

5.5. Binding free energy analysis

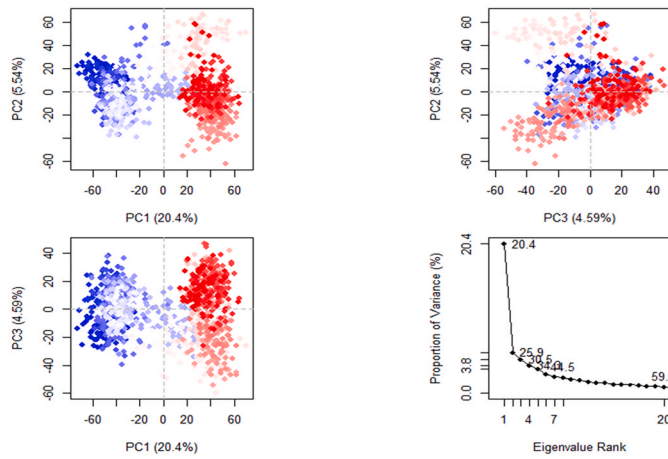
To evaluate the molecular binding interaction of protein-ligand complexes, the binding free energy (Δ G) was computed using MM-PBSA, which accounts for the bonded and non-bonded (van der Waals and electrostatic) interactions. The binding free energies of the protein-ligand complexes were determined by employing MM-PBSA and the final 50 ns of the trajectory. Table 4, and Fig. 11 summarize the major components of binding free energy for protein-ligand complexes, including van der Waals (Δ EVDW), electrostatics (Δ EEEL), a polar portion of solvation (Δ GPB), nonpolar part of solvation (Δ GNP), dispersion (Δ GDISP), and binding energy (Δ G).

In Fig. 11, it shows that sarsapogenin has the highest binding energy compared to Diosgenin and standard Mitomycin. Additionally, energy factors, together with van der Waals strength and the nonpolar part of solvation-loose strength, are giant members of the overall binding-loose power of the complexes. Compared to the value of the GPB component, the value of WDW is negative, indicating non-polar interactions between the protein-ligand complexes.

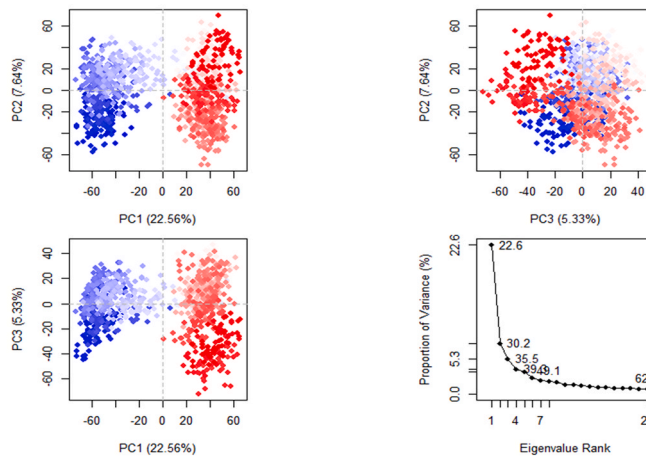
Finally, by using a protein dynamics analysis tool known as PCA, it is possible to obtain a series of eigenvalues and eigenvectors that reflect the overall motion of the protein. Additionally, the method can be used to study the influence of different parameters on the collective movement and to simplify the movement, which is related to the system's stability and protein function. In addition, it may be used to characterize the various conformational variances involved in the process of protein folding and ion channel open-close mechanisms. The conformation changes in the protein backbone were ascertained by principal component analysis (PCA). The first three PCs predicted the majority of the motion of the protein backbone from the MD trajectories in Fig. 12. In the Diosgenin protein, PCA analysis shows that the first three eigenvectors account for 19.03 %, 19.03 %, and 6.33 % (Fig. 12A). In the case of Sarsasapogenin



A. Diosgenin



B. Sarsasapogenin



C. Standard Mitomycin

(caption on next page)

Fig. 12. Principal component analysis (PCA).

with Protein, PCA analysis displays that the first three eigenvectors account for 20.4 %, 20.4 %, and 4.59 % (Fig. 12B). In the case of standard Protein, PCA analysis displays that the first three eigenvectors account for 22.56 %, 22.56 %, and 5.33 % (Fig. 12C). The highest PC1 (22.56 %) was noticed for standard protein, which indicates that the protein had undergone greater conformational changes. Conversely, the lowest PC1 (4.59 %) was observed for the Sarsa protein, indicating that the protein had undergone very few conformational changes.

The results of PCA including PC2 vs PC1, PC2 vs PC3, and PC3 vs PC1 colored from blue to red in order of time, and an eigenvalue rank plot for Diosgenin, Sarsa, and standard, respectively (Fig. 12). The cumulative variance is labeled for each data point in the eigenvalue plot.

5.6. ADMET data investigation

We have prioritized parameters like water solubility, Caco-2 permeability, and human intestinal absorption for comparative absorption analysis of these compounds. For any drug-like compound, calculating water solubility can be an important parameter as it directly correlates positively with the absorption of that specific drug in our system. pkCSM estimated the water solubility of all nine compounds at 25 °C and represented the data in Log S. According to the Log S Scale: insoluble < -10 poorly < -6, moderately < -4 soluble < -2 very < 0 < highly [77–79]. As stated in Table 5, compounds 16, 25, and 26 were poorly soluble, whereas compounds 04, 05, 07, 10, and 11 were either soluble or moderately soluble. On the other hand, for assessing human intestine absorption, compounds 07 and 11 showed 100 % absorption, whereas the standard compound mitomycin had an absorption of 69.834 %. Only two compounds (05 and 10) had a lower absorption score than the standard drug. Human colorectal adenocarcinoma epithelial cells are responsible for the Caco-2 cell line, which is commonly used as a valid model to examine the absorption property of any orally administered drugs [80]. As stated in the pkCSM guideline Caco-2 permeability value over 0.9 is considered high Caco-2 permeability. Compounds 04, 05, 25 and 26 expressed higher Caco-2 permeability than Mitomycin, and compound 16 represented the lowest Caco-2 permeability value.

Concerning the distribution of elected compounds were subjected to calculate crucial aspects like the volume of distribution (VD_{ss}) and blood-brain barrier (BBB). The VD values suggest whether or not medicines are distributed evenly between blood and tissue. A higher VD score (>0.45) implies that the therapeutic molecule is more smoothly distributed in the tissue rather than plasma, and a lower (<-0.15) value indicates the poor distribution of the substance in tissues. Mitomycin has a VD_{ss} value of -0.132, but compound 03 and 07 revealed a higher VD_{ss} value than the standard compound, which suggests their better distribution in tissue than blood plasma. BBB protects our brain from interacting with any external compounds. As a result, the ability of any drug to cross BBB could be a vital parameter. BBB permeability score of < -1 indicates poor distribution. Inversely, a score of >0.3 expresses excellent BBB permeability. The BBB permeability was interpreted by compound 03. Alternately the minimum BBB permeability score was expressed by compound 05. Cytochrome P450, present in the human liver, belongs to the group of detoxification enzymes that plays a significant role in drug metabolism [81]. Several drugs can inhibit Cytochrome P450. Therefore, it is extremely decisive to assess the ability of the compounds to inhibit this enzyme. In our study, we have calculated the inhibition value for two isoforms (CYP450 1A2 and CYP450 2D6) of Cytochrome P450. Table 5 shows none of the compounds inhibited CYP450 1A2 except compounds 04 and 07. However, CYP450 2D6 has been predicted to be inhibited by compound 03, and all other compounds were predicted to lack the ability to inhibit CYP450 2D6.

Excretion analysis was incorporated by estimating total clearance and Organic Cation Transporter 2 (OCT2). The total release uses the combined data of hepatic and renal clearance to obtain a total clearance score that gives a clear excretion profile of any specific drug [82]. By analyzing total clearance data from Tables 5 and it can be stated that compounds 03 and 06 have better total clearance values than Mitomycin. By comparison, the compound had the maximum, and compound 11 had the lowest total clearance value. OCT2 is a renal intake transporter that plays a critical role in the renal clearance of drugs and external compounds. Except for compound 25, all other compounds were predicted to have a potential positive correlation to work as a substrate for the OCT2 enzyme. Similarly, toxicity data were also predicted using the pkCSM tool, where none of the suggested compounds were found to be involved in skin sensitization and hepatotoxicity. We should assume from these estimated ADMET values that the compounds suggested in our investigation have suitable physicochemical characteristics and decent drug-likeness, making them potential treatment options.

6. Discussion

H. pylori disrupts cell proliferation and apoptosis by introducing virulence factors such as CagA, VacA, LPS, and Tip α , with the latter playing a crucial role in inducing Epithelial-Mesenchymal Transition (EMT) in gastric cancer. Tip α , released by *H. pylori* strains from gastric cancer patients, binds to cell surface nucleoli receptors and stimulates EMT marker expression, promoting metastatic gastric cancer through gene expression and morphological changes. Interestingly, researchers found Lpp20, another *H. pylori* protein sharing structural similarities with Tip α , to activate NF- κ B and induce EMT. Both Tip α and Lpp20 enhance cell migration and down-regulate E-cadherin, leading to metastatic gastric cancer development. Given their significance in gastric cancer progression, this study targets Tip α (PDB ID: 3GUQ) and Lpp20 (PDB ID: 5OK8) as potential drug targets, employing computational approaches for designing effective therapeutic molecules.

Earlier data reported that the mentioned compounds have various pharmacological effects. Still, no study is available against gastric cancer associated with *H. pylori*. That's why, the mentioned natural compounds have been selected for the present study and

Table 5

ADMET data of selected eight compounds along with standard compound Mitomycin.

S/N	Absorption			Distribution		Metabolism		Excretion		Toxicity	
	Water solubility Log S	Caco-2 Permeability x 10 ⁻⁶	Human Intestinal Absorption (%)	VDss (human)	BBB Permeability	CYP450 1A2 Inhibitor	CYP450 2D6 substrate	Total Clearance (ml/min/kg)	Renal OCT2 substrate	Skin Sensitization	Hepatotoxicity
04	-3.862	1.292	94.957	0.116	No	Yes	No	0.222	No	No	No
05	-3.589	0.415	29.808	-0.377	No	No	No	0.213	No	No	No
07	-4.485	1.302	100	1.302	Yes	Yes	Yes	1.069	No	No	No
10	-3.339	0.552	39.685	-0.535	No	No	No	0.467	No	No	No
11	-3.419	0.883	100	-1.105	Yes	No	No	-0.114	No	No	No
16	-6.074	0.053	86.841	-0.676	No	No	No	2.147	No	No	No
25	-6.151	1.227	98.329	0.466	Yes	No	No	0.324	Yes	No	No
26	-6.213	1.228	98.483	0.286	No	No	No	0.318	No	No	No
Mitomycin	-3.226	0.59	69.834	-0.132	No	No	No	0.862	No	No	Yes

implemented advanced *in silico* investigation to determine the possible pharmacological activity against targeted protein. The study analyses ADMET, drug-likeness, molecular docking, binding free energy calculation, and molecular dynamic simulation for selected compounds. Through analyzing the findings obtained from mentioned approaches, it can be suggested that the majority of our selected compounds, including Glabridin, Sanguinarine, Glycyrrhetic acid, Beta-carotin, Diosgenin, Sarsasapogenin, were found to be potentially effective in inhibiting the targeted receptors Lpp20 (HP1456) from *H. pylori* (PDB ID: 5OK8), and *H. pylori*-carcinogenic, and TNF-alpha-inducing protein (PDB ID3GUQ) which reflecting their promising role for the treatment of gastric cancer in particular caused by *H. pylori* infection. Most of the molecules analyzed revealed better absorption rates and aqueous solubility while showing minimal toxic effects.

Accumulated evidence and epidemiological investigations have reflected that natural product, including phytochemicals, have been explored potentially for the prevention and treatment of cancers and found to be useful in developing drugs and medicines counteracting and managing cancers, including gastric cancer caused by *H. pylori* infection [17,19,20,83]. Notably, various studies have suggested that mentioned bioactive phytochemical components with structural stability, potential bioavailability, and bioactivity could play a crucial role in formulating novel treatment regimens for gastric cancer management while minimizing the adverse effects associated with chemotherapeutic drugs as well as being comparatively safer. Experimental studies have thrown some light on the mechanisms of action, such as suppressing angiogenesis, inhibiting cancer cell proliferation, inducing apoptosis and autophagy, and cancer cell metastasis, which have also been found to be associated with inhibiting *H. pylori* as well as modulating the gut microbiota to produce anti-bacterial and anti-cancer activities additionally. Moreover, clinical studies have also proven to some extent that phytochemicals possess the potential for the prevention and management of gastric cancer in humans. Of note, more researches, explorative studies, and investing actions are of utmost need to a for better understanding of the underlying mechanisms of cancer treatment utilizing phytochemicals, knowing possible side effects, and promoting this approach to its full practical potential in ameliorating gastric cancer and *H. pylori* infection as well as a cost-effective complementary and combination approach [14,16,84].

7. Conclusion

Our innovative study employing computer-aided drug design has unraveled promising compounds against *H. pylori*, a bacterium intricately linked to various gastrointestinal ailments, including the formidable gastric cancer. The binding affinities observed for *H. pylori*-associated TNF-alpha-inducing protein and Lpp20 with values as -9.4 kcal/mol and -9.2 kcal/mol, respectively, signal strong potential for therapeutic intervention. Furthermore, these natural compounds exhibit favorable pharmacokinetic properties, such as enhanced absorption rates and solubility, coupled with low toxicity profiles. These attributes underscore the promise of these phytochemicals as effective combatants against *H. pylori*-induced gastrointestinal disorders.

As we steer into the future, there's an enthralling avenue worth exploring: the application of PROTACs (PROteolysis Targeting Chimeras). PROTACs, by virtue of their ability to induce selective degradation of target proteins, could significantly augment the therapeutic efficacy and specificity of the identified molecules against *H. pylori*. By harnessing the potential of PROTACs, we might be able to design treatments that not only inhibit the activity but also lead to the degradation of harmful *H. pylori* proteins. The world stands on the cusp of potentially revolutionary treatments against *H. pylori* and its associated maladies. As we conclude, we ardently advocate for accelerated research into these promising phytochemicals. It's crucial to propel them from computer models to laboratory benches and finally to the patient's bedside. With in-depth *in vitro*, *in vivo*, and clinical studies, we envision a future where the global burden of *H. pylori* is significantly diminished, and the journey towards safer, nature-derived drugs is paved.

Data availability statement

All data used to support the findings of this study are included in the article.

Ethics approval

Not applicable.

Declaration of competing interest

The authors declare that they have no known competing financial interests or personal relationships that could have appeared to influence the work reported in this paper.

Acknowledgment

The authors extend their appreciation to the Researchers Supporting Project number (RSPD2023R758), King Saud University, Riyadh, Saudi Arabia.

Appendix A. Supplementary data

Supplementary data to this article can be found online at <https://doi.org/10.1016/j.heliyon.2023.e20670>.

References

- [1] M. Fiorani, et al., The influence of *Helicobacter pylori* on human gastric and gut microbiota, *Antibiotics* 12 (4) (2023) 765, <https://doi.org/10.3390/antibiotics12040765>.
- [2] J. Wideliski, et al., Correlation between chemical profile of Georgian propolis extracts and their activity against *Helicobacter pylori*, *Molecules* 28 (3) (2023) 1374, <https://doi.org/10.3390/molecules28031374>.
- [3] Y. Li, et al., Global Prevalence of *Helicobacter pylori* Infection between 1980 and 2022: a Systematic Review and Meta-Analysis, *The Lancet Gastroenterology & Hepatology*, 2023. [https://www.thelancet.com/journals/langas/article/PIIS2468-1253\(23\)00070-5/fulltext](https://www.thelancet.com/journals/langas/article/PIIS2468-1253(23)00070-5/fulltext).
- [4] H. Yang, et al., The role of adhesion in *Helicobacter pylori* persistent colonization, *Curr. Microbiol.* 80 (5) (2023) 185. <https://link.springer.com/article/10.1007/s00284-023-03264-6>.
- [5] M. Alsina, M. Diez, J. Tabernero, Emerging biological drugs for the treatment of gastroesophageal adenocarcinoma, *Expert Opin. Emerg. Drugs* 26 (4) (2021) 385–400, <https://doi.org/10.1080/14728214.2021.2010705>.
- [6] S.I. Smith, et al., *Helicobacter pylori* infection in Africa: update of the current situation and challenges, *Dig. Dis.* 40 (4) (2022) 535–544, <https://doi.org/10.1159/000518959>.
- [7] N.J. Talley, K.M. Fock, P. Moayyedi, Gastric Cancer Consensus conference recommends *Helicobacter pylori* screening and treatment in asymptomatic persons from high-risk populations to prevent gastric cancer, *Offl. J. Am. College Of Gastroenterol.* | ACG 103 (3) (2008) 510–514. https://journals.lww.com/ajg/Abstract/2008/03000/Gastric_Cancer_Consensus_Conference_Recommends.2.aspx.
- [8] N. Aumpun, V. Mahachai, R.K. Vilaichone, Management of *Helicobacter pylori* infection, *JGH Open* 7 (1) (2023) 3–15, 10.1002/jgh3.12843.
- [9] G. Pappas-Gogos, et al., The implication of gastric microbiome in the treatment of gastric cancer, *Cancers* 14 (8) (2022) 2039, 10.3390/cancers14082039.
- [10] K.S.-H. Liu, I.O.-L. Wong, W.K. Leung, *Helicobacter pylori* associated gastric intestinal metaplasia: treatment and surveillance, *World J. Gastroenterol.* 22 (3) (2016) 1311. <https://www.ncbi.nlm.nih.gov/pmc/articles/PMC4716041/>.
- [11] Q. Cai, et al., Inflammation-associated senescence promotes *Helicobacter pylori*-induced atrophic gastritis, *Cellular and Mol. Gastroenterol. Hepatol.* 11 (3) (2021) 857–880, 10.1016/j.jcmgh.2020.10.015.
- [12] M. Talebi, et al., Therapeutic effects of resveratrol in inflammatory bowel diseases: shedding light on the role of cellular and molecular pathways, *Revista Brasileira de Farmacognosia* 32 (2) (2022) 160–173. <https://link.springer.com/article/10.1007/s43450-022-00247-9>.
- [13] U. Thalmaier, et al., Role of tumor necrosis factor alpha in *Helicobacter pylori* gastritis in tumor necrosis factor receptor 1-deficient mice, *Infect. Immun.* 70 (6) (2002) 3149–3155, <https://doi.org/10.1128/iai.70.6.3149-3155.2002>.
- [14] S.-H. Park, et al., Non-microbial approach for *Helicobacter pylori* as faster track to prevent gastric cancer than simple eradication, *World J. Gastroenterol.*: WJG 19 (47) (2013) 8986, <https://doi.org/10.3748/wjg.v19.i47.8986>.
- [15] A. Ghasemian, et al., Herbal medicine as an auspicious therapeutic approach for the eradication of *Helicobacter pylori* infection: a concise review, *J. Cell. Physiol.* 234 (10) (2019) 16847–16860, 10.1002/jcp.28363.
- [16] S. Sathianarayanan, et al., A new approach against *Helicobacter pylori* using plants and its constituents: a review study, *Microb. Pathog.* (2022), 105594, <https://doi.org/10.1016/j.micpath.2022.105594>.
- [17] S.Y. Kang, et al., Potential of bioactive food components against gastric cancer: insights into molecular mechanism and therapeutic targets, *Cancers* 13 (18) (2021) 4502, 10.3390/cancers13184502.
- [18] Y. Ai, et al., Pull the plug: anti-angiogenesis potential of natural products in gastrointestinal cancer therapy, *Phytother Res.* 36 (9) (2022) 3371–3393, 10.1002/ptr.7492.
- [19] Q.-Q. Mao, et al., Phytochemicals for the prevention and treatment of gastric cancer: effects and mechanisms, *Int. J. Mol. Sci.* 21 (2) (2020) 570, 10.3390/ijms21020570.
- [20] R.K. Al-Ishaq, A.J. Overy, D. Büsselberg, Phytochemicals and gastrointestinal cancer: cellular mechanisms and effects to change cancer progression, *Biomolecules* 10 (1) (2020) 105, 10.3390/biom10010105.
- [21] H. Yuan, et al., The traditional medicine and modern medicine from natural products, *Molecules* 21 (5) (2016) 559, 10.3390/molecules21050559.
- [22] W.M. Bandaranayake, *Quality Control, Screening, Toxicity, and Regulation of Herbal Drugs*. Modern Phytomedicine: Turning Medicinal Plants into Drugs, 2006, pp. 25–57. <https://onlinelibrary.wiley.com/doi/book/10.1002/9783527609987#page=45>.
- [23] M. Goel, et al., Efficient and enhanced sampling of drug-like chemical space for virtual screening and molecular design using modern machine learning methods, *Wiley Interdiscip. Rev. Comput. Mol. Sci.* 13 (2) (2023) e1637, 10.1002/wcms.1637.
- [24] C. Simmler, G.F. Pauli, S.-N. Chen, Phytochemistry and biological properties of glabridin, *Fitoterapia* 90 (2013) 160–184, <https://doi.org/10.1016/j.fitote.2013.07.003>.
- [25] Z. Yang, et al., Glabridin inhibits urothelial bladder carcinoma cell growth in vitro and in vivo by inducing cell apoptosis and cell cycle arrest, *Chem. Biol. Drug Des.* (2022), <https://doi.org/10.1111/cbdd.14147>.
- [26] C.-x. Li, et al., Pharmacological properties of glabridin (a flavonoid extracted from licorice): a comprehensive review, *J. Funct. Foods* 85 (2021), 104638, <https://doi.org/10.1016/j.jff.2021.104638>.
- [27] C. Yu, et al., Serotonergically dependent antihyperalgesic and antiallodynic effects of isoliquiritin in a mouse model of neuropathic pain, *Eur. J. Pharmacol.* 881 (2020), 173184, <https://doi.org/10.1016/j.ejphar.2020.173184>.
- [28] A. Kim, J.Y. Ma, Isoliquiritin apioside suppresses in vitro invasiveness and angiogenesis of cancer cells and endothelial cells, *Front. Pharmacol.* 9 (2018) 1455, <https://doi.org/10.3389/fphar.2018.01455>.
- [29] J. Wang, et al., Isoliquiritin modulates ferroptosis via NF- κ B signalling inhibition and alleviates doxorubicin resistance in breast cancer, *Immunopharmacol. Immunotoxicol.* (2023) 1–17, <https://doi.org/10.1080/08923973.2023.2165943> (just-accepted).
- [30] C.K. Singh, et al., Molecular signatures of sanguinarine in human pancreatic cancer cells: a large scale label-free comparative proteomics approach, *Oncotarget* 6 (12) (2015), 10335, <https://doi.org/10.18632/oncotarget.3231>.
- [31] R. Zhang, et al., Sanguinarine inhibits growth and invasion of gastric cancer cells via regulation of the DUSP4/ERK pathway, *J. Cell Mol. Med.* 21 (6) (2017) 1117–1127, 10.1111/jcmm.13043.
- [32] H.-N. Fan, et al., Sanguinarine inhibits the tumorigenesis of gastric cancer by regulating the TOX/DNA-PKcs/KU70/80 pathway, *Pathol. Res. Pract.* 215 (11) (2019), 152677, <https://doi.org/10.1016/j.prp.2019.152677>.
- [33] L. Teng, et al., Liquiritin modulates ERK-and AKT/GSK-3 β -dependent pathways to protect against glutamate-induced cell damage in differentiated PC12 cells, *Mol. Med. Rep.* 10 (2) (2014) 818–824, <https://doi.org/10.3892/mmr.2014.2289>.
- [34] J. Qin, et al., Pharmacological activities and pharmacokinetics of liquiritin: a review, *J. Ethnopharmacol.* 293 (2022), 115257, <https://doi.org/10.1016/j.jep.2022.115257>.
- [35] J.M. Hendricks, et al., 18 β -glycyrrhetic acid delivered orally induces isolated lymphoid follicle maturation at the intestinal mucosa and attenuates rotavirus shedding, *PLoS One* 7 (11) (2012), e49491, <https://doi.org/10.1371/journal.pone.0049491>.
- [36] X.-F. Wang, et al., Glycyrrhetic acid potently suppresses breast cancer invasion and metastasis by impairing the p38 MAPK-AP1 signaling axis, *Expert Opin. Ther. Targets* 19 (5) (2015) 577–587, <https://doi.org/10.1517/14728222.2015.1012156>.
- [37] D. Lin, et al., Involvement of BID translocation in glycyrrhetic acid and 11-deoxy glycyrrhetic acid-induced attenuation of gastric cancer growth, *Nutr. Cancer* 66 (3) (2014) 463–473, <https://doi.org/10.1080/01635581.2013.877498>.
- [38] L.J. Johnson, S.L. Meacham, L.J. Kruskall, The antioxidants-vitamin C, vitamin E, selenium, and carotenoids, *J. Agromed.* 9 (1) (2003) 65–82, https://doi.org/10.1300/J096v09n01_07.
- [39] M. Musayev, Agro-ecological characteristics of sea buckthorn (*Hippophae rhamnoides* L.) in Azerbaijan, *J. Crop Weed* 9 (2013) 114–120. <https://www.cropandweed.com/vol9issue1/pdf2005/19.pdf>.

- [40] S. Kasperczyk, et al., Beta-carotene reduces oxidative stress, improves glutathione metabolism and modifies antioxidant defense systems in lead-exposed workers, *Toxicol. Appl. Pharmacol.* 280 (1) (2014) 36–41, <https://doi.org/10.1016/j.taap.2014.07.006>.
- [41] G.S. Omenn, et al., Effects of a combination of beta carotene and vitamin A on lung cancer and cardiovascular disease, *N. Engl. J. Med.* 334 (18) (1996) 1150–1155, <https://doi.org/10.1056/NEJM199605023341802>.
- [42] M. Jesus, et al., Diosgenin: recent highlights on pharmacology and analytical methodology, *J. Anal. Meth. Chem.* (2016), <https://doi.org/10.1155/2016/4156293>, 2016.
- [43] J. Lee, et al., Diosgenin inhibits melanogenesis through the activation of phosphatidylinositol-3-kinase pathway (PI3K) signaling, *Life Sci.* 81 (3) (2007) 249–254, <https://doi.org/10.1016/j.lfs.2007.05.009>.
- [44] Z.-J. Mao, et al., Anti-proliferation and anti-invasion effects of diosgenin on gastric cancer BGC-823 cells with HIF-1 α shRNAs, *Int. J. Mol. Sci.* 13 (5) (2012) 6521–6533, [10.3390/ijms13056521](https://doi.org/10.3390/ijms13056521).
- [45] C. Nie, et al., Diosgenin-induced autophagy and apoptosis in a human prostate cancer cell line, *Mol. Med. Rep.* 14 (5) (2016) 4349–4359, <https://doi.org/10.3892/mmr.2016.5750>.
- [46] W. Wang, et al., Novel sarsasapogenin-triazolyl hybrids as potential anti-Alzheimer's agents: design, synthesis and biological evaluation, *Eur. J. Med. Chem.* 151 (2018) 351–362, <https://doi.org/10.1016/j.ejmech.2018.03.082>.
- [47] D. Dong, et al., Sarsasapogenin-AA13 inhibits LPS-induced inflammatory responses in macrophage cells in vitro and relieves dimethylbenzene-induced ear edema in mice, *Acta Pharmacol. Sin.* 38 (5) (2017) 699–709, <https://www.nature.com/articles/aps2016180>.
- [48] W. Wang, et al., Synthesis of new sarsasapogenin derivatives with cytotoxicity and apoptosis-inducing activities in human breast cancer MCF-7 cells, *Eur. J. Med. Chem.* 127 (2017) 62–71, <https://doi.org/10.1016/j.ejmech.2016.12.011>.
- [49] Y. Ni, et al., Mitochondrial ROS burst as an early sign in sarsasapogenin-induced apoptosis in HepG2 cells, *Cell Biol. Int.* 32 (3) (2008) 337–343, <https://doi.org/10.1016/j.cellbi.2007.12.004>.
- [50] C.A. Lipinski, 4, Lead-and Drug-Like Compounds: The Rule-of-Five Revolution, 1, 2004, pp. 337–341, <https://doi.org/10.1016/j.ddtec.2004.11.007>.
- [51] W.P. Walters, A.A. Murcko, M.A. Murcko, Recognizing Molecules With Drug-Like Properties, 3, 1999, pp. 384–387, [https://doi.org/10.1016/S1367-5931\(99\)80058-1](https://doi.org/10.1016/S1367-5931(99)80058-1) (4).
- [52] B. Bakchi, et al., An overview on applications of SwissADME web tool in the design and development of anticancer, antitubercular and antimicrobial agents: a medicinal chemist's perspective, *J. Mol. Struct.* (2022), 132712, <https://doi.org/10.1016/j.molstruc.2022.132712>.
- [53] A. Daina, O. Michielin, V.J.S.R. Zoete, 1, Swissadme: A Free Web Tool To Evaluate Pharmacokinetics, Drug-Likeness And Medicinal Chemistry Friendliness Of Small Molecules, 7, 2017, pp. 1–13, <https://www.nature.com/articles/srep42717>.
- [54] A. Kumer, et al., 4, The Computational Screening Of Inhibitor For Black Fungus And White Fungus By D-Glucufuranose Derivatives Using In Silico And Sar Study, 14, 2021, <https://doi.org/10.25135/acg.oc.116.2108.2188>.
- [55] P. Ertl, B. Rohde, P. Selzer, 20, Fast Calculation of Molecular Polar Surface Area as a Sum of Fragment-based Contributions and its Application to the Prediction of Drug Transport Properties, 43, 2000, pp. 3714–3717, <https://doi.org/10.1021/jm000942e>.
- [56] Y.C.J. Martin, A Bioavail. Sec 48 (9) (2005) 3164–3170, <https://doi.org/10.1021/jm0492002>.
- [57] A.P. Li, 7, Screening For Human Adme/Tox Drug Properties in Drug Discovery, 6, 2001, pp. 357–366, [https://doi.org/10.1016/S1359-6446\(01\)01712-3](https://doi.org/10.1016/S1359-6446(01)01712-3).
- [58] D.E. Pires, T.L. Blundell, D.B. Ascher, 9, Pkcsim: Predicting Small-Molecule Pharmacokinetic And Toxicity Properties Using Graph-Based Signatures, 58, 2015, pp. 4066–4072, <https://doi.org/10.1021/acs.jmedchem.5b00104>.
- [59] L. Guo, et al., 7, A Comparison Of Various Optimization Algorithms Of Protein-Ligand Docking Programs By Fitness Accuracy, 20, 2014, pp. 1–10, <https://link.springer.com/article/10.1007/s00894-014-2251-3>.
- [60] D. Sibanda, S.T. Oyibo, T.-C. Jen, A review of atomic layer deposition modelling and simulation methodologies: density functional theory and molecular dynamics, *Nanotechnol. Rev.* 11 (1) (2022) 1332–1363, <https://doi.org/10.1515/ntrev-2022-0084>.
- [61] S.K. Burley, et al., D1, Rcsb Protein Data Bank: Biological Macromolecular Structures Enabling Research And Education In Fundamental Biology, Biomedicine, Biotechnology And Energy, 47, 2019, pp. D464–D474, <https://doi.org/10.1093/nar/gky1004>.
- [62] H. Tsuge, et al., Structural basis for the Helicobacter pylori-carcinogenic TNF- α -inducing protein, *Biochem. Biophys. Res. Commun.* 388 (2) (2009) 193–198, <https://doi.org/10.1016/j.bbrc.2009.07.121>.
- [63] F. Vallese, et al., Helicobacter pylori antigenic Lpp20 is a structural homologue of Tip α and promotes epithelial-mesenchymal transition, *Biochim. Biophys. Acta, Gen. Subj.* 1861 (12) (2017) 3263–3271, <https://doi.org/10.1016/j.bbagen.2017.09.017>.
- [64] E. Chrobak, et al., Molecular structure, in vitro anticancer study and molecular docking of new phosphate derivatives of betulin, *Molecules* 26 (3) (2021) 737, [10.3390/molecules26030737](https://doi.org/10.3390/molecules26030737).
- [65] S. Dallakyan, A.J. Olson, Small-molecule Library Screening by Docking with PyRx. *Chemical Biology: Methods and Protocols*, 2015, pp. 243–250. https://link.springer.com/protocol/10.1007/978-1-4939-2269-7_19.
- [66] P.T. Rangisetty, et al., RSAD2: an exclusive target protein for Zika virus comparative modeling, characterization, energy minimization and stabilization, *Int. J. Health Sci.* 17 (1) (2023) 12–17, <https://www.ncbi.nlm.nih.gov/pmc/articles/PMC9832909/>.
- [67] M. Kurki, et al., Structure of POPC lipid bilayers in OPLS3e force field, *J. Chem. Inf. Model.* 62 (24) (2022) 6462–6474, <https://doi.org/10.1021/acs.jcim.2c00395>.
- [68] T.U. da Silva, et al., Development of parameters compatible with the CHARMM36 force field for [Fe4S4]²⁺ clusters and molecular dynamics simulations of adenosine-5'-phosphosulfate reductase in GROMACS 2019, *J. Biomol. Struct. Dyn.* 40 (8) (2022) 3481–3491, <https://doi.org/10.1080/07391102.2020.1847687>.
- [69] W. Humphrey, A. Dalke, K. Schulten, VMD: visual molecular dynamics, *J. Mol. Graph.* 14 (1) (1996) 33–38, [https://doi.org/10.1016/0263-7855\(96\)00018-5](https://doi.org/10.1016/0263-7855(96)00018-5).
- [70] B.R. Miller III, et al., MMPBSA.py: an efficient program for end-state free energy calculations, *J. Chem. Theor. Comput.* 8 (9) (2012) 3314–3321, <https://doi.org/10.1021/ct300418h>.
- [71] H. Sun, et al., Assessing the performance of MM/PBSA and MM/GBSA methods. 7. Entropy effects on the performance of end-point binding free energy calculation approaches, *Phys. Chem. Chem. Phys.* 20 (21) (2018) 14450–14460, [10.1039/C7CP07623A](https://doi.org/10.1039/C7CP07623A).
- [72] N. Kumar, et al., Structure-based virtual screening, molecular dynamics simulation and MM-PBSA toward identifying the inhibitors for two-component regulatory system protein NarL of Mycobacterium Tuberculosis, *J. Biomol. Struct. Dyn.* 38 (11) (2020) 3396–3410, <https://doi.org/10.1080/07391102.2019.1657499>.
- [73] W.P. Walters, Going further than Lipinski's rule in drug design, *Expert Opin. Drug Discov.* 7 (2) (2012) 99–107, <https://doi.org/10.1517/17460441.2012.648612>.
- [74] A. Nadin, C. Hattotuwa, I. Churcher, Lead-oriented synthesis: a new opportunity for synthetic chemistry, *Angew. Chem. Int. Ed.* 51 (5) (2012) 1114–1122, [10.1002/anie.201105840](https://doi.org/10.1002/anie.201105840).
- [75] A. Nath, et al., Investigating the binding affinity, molecular dynamics, and ADMET properties of 2, 3-dihydrobenzofuran derivatives as an inhibitor of fungi, bacteria, and virus protein, *Beni-Suef Univ. J. Basic and Appl. Sci.* 10 (1) (2021) 1–13, <https://bjbas.springeropen.com/articles/10.1186/s43088-021-00117-8>.
- [76] S.R. Mahapatra, et al., The potential of plant-derived secondary metabolites as novel drug candidates against Klebsiella pneumoniae: molecular docking and simulation investigation, *South Afr. J. Bot.* 149 (2022) 789–797, <https://doi.org/10.1016/j.sajb.2022.04.043>.
- [77] B. Debnath, S. Ganguly, 3, Synthesis, Biological Evaluation, In Silico Docking, And Virtual Adme Studies Of 2-[2-Oxo-3-(Arylimino) Indolin-1-Yl]-N-Arylacetamides As Potent Anti-Breast Cancer Agents, 147, 2016, pp. 565–574, <https://link.springer.com/article/10.1007/s00706-015-1566-9>.
- [78] C.A. Lipinski, 1, Drug-Like Properties and the Causes of Poor Solubility and Poor Permeability, 44, 2000, pp. 235–249, [https://doi.org/10.1016/S1056-8719\(00\)00107-6](https://doi.org/10.1016/S1056-8719(00)00107-6).
- [79] C.A. Lipinski, et al., 1–3, Experimental And Computational Approaches To Estimate Solubility And Permeability In Drug Discovery And Development Settings, 23, 1997, pp. 3–25, <https://doi.org/10.1016/j.addr.2012.09.019>.

- [80] K. Verhoeckx, et al., The Impact of Food Bioactives on Health: in Vitro and Ex Vivo Models, 2015. <https://library.oapen.org/bitstream/handle/20.500.12657/28028/1001968.pdf>.
- [81] C.C. Ogu, J.L. Maxa, Drug interactions due to cytochrome P450, in: Baylor University Medical Center Proceedings, Taylor & Francis, 2000, <https://doi.org/10.1080/08998280.2000.11927719>.
- [82] F.J. Dowd, et al., Pharmacology and Therapeutics for Dentistry-E-Book, Elsevier Health Sciences, 2010. <https://evolve.elsevier.com/cs/product/9780323168304?role=student>.
- [83] Z. Liang, et al., Anticancer applications of phytochemicals in gastric cancer: effects and molecular mechanism, Front. Pharmacol. 13 (2022), <https://doi.org/10.3389/fphar.2022.1078090>.
- [84] B. Rizeq, et al., The power of phytochemicals combination in cancer chemoprevention, J. Cancer 11 (15) (2020) 4521–4533, <https://doi.org/10.7150/jca.34374>.